Aalborg Universitet

Modeling and Control of Solid-State Synchronous Generator

Chen, Meng

DOI (link to publication from Publisher):
10.54337/aau460278660

Publication date:
2021

Document Version
Publisher's PDF, also known as Version of record

Link to publication from Aalborg University

Citation for published version (APA):
Chen, M. (2021). *Modeling and Control of Solid-State Synchronous Generator*. Aalborg Universitetsforlag.

General rights
Copyright and moral rights for the publications made accessible in the public portal are retained by the authors and/or other copyright owners and it is a condition of accessing publications that users recognise and abide by the legal requirements associated with these rights.

- Users may download and print one copy of any publication from the public portal for the purpose of private study or research.
- You may not further distribute the material or use it for any profit-making activity or commercial gain
- You may freely distribute the URL identifying the publication in the public portal -

Take down policy
If you believe that this document breaches copyright please contact us at vbn@aub.aau.dk providing details, and we will remove access to the work immediately and investigate your claim.

Downloaded from vbn.aau.dk on: December 06, 2025

MODELING AND CONTROL OF SOLID-STATE SYNCHRONOUS GENERATOR

BY
MENG CHEN

DISSERTATION SUBMITTED 2021

AALBORG UNIVERSITY
DENMARK

Modeling and Control of Solid-State Synchronous Generator

Ph.D. Dissertation

Meng Chen

Dissertation submitted September, 2021

Dissertation submitted: September, 2021

PhD supervisor: Prof. Frede Blaabjerg
Aalborg University, Denmark

Assistant PhD supervisor: Assoc. Prof. Dao Zhou
Aalborg University, Denmark

PhD committee: Professor Birgitte Bak-Jensen
Aalborg University

Associate Professor Jon Are Wold Suul
Norwegian University of Science and Technology

Professor George Weiss
Tel Aviv University

PhD Series: Faculty of Engineering and Science, Aalborg University

Department: Department of Energy Technology

ISSN (online): 2446-1636
ISBN (online): 978-87-7210-854-4

Published by:
Aalborg University Press
Kroghstræde 3
DK – 9220 Aalborg Ø
Phone: +45 99407140
aauf@forlag.aau.dk
forlag.aau.dk

© Copyright: Meng Chen

Printed in Denmark by Rosendahls, 2021

Abstract

Solid-state synchronous generator (SSSG), namely virtual synchronous generator (VSG), is a promising way to integrate inverter-interfaced generators (IIGs) into the power system. Nevertheless, differences in modeling, control, and application between the SSSG and synchronous generator (SG) pose new challenging issues for the stable operation of the power system with SSSGs.

Firstly, various models used for an SSSG to emulate an SG inevitably lead to different characteristics of the power system. Meanwhile, the structure of the power system itself is becoming more distributed and may not be strong as usual. The existing analysis of an SG such as based on a single-machine-infinite-bus (SMIB) system can not provide a comprehensive evaluation on the SSSG. Thus, further detailed characteristics analysis of the SSSG is necessary.

Secondly, a power-electronic-based SSSG provides the possibility of adding more favorable features, which an SG does not internally have in order to provide a superior and robust performance by advanced control algorithm. Meanwhile, in order to optimize the performance of the SSSG, the coupling among several control loops should also be taken care of. Therefore, the advanced control is of importance to fully take advantages of the power-electronic-based SSSG.

To cope with the aforementioned issues, this Ph.D. project investigates the characteristics analysis and advanced control of the SSSG. Specifically, various modelings of SSSG are compared with each other and also with the SG. Further, the impact of the SSSG on the electromechanical oscillation is studied in details by using a small-signal and participation factor analysis. How the SSSG changes the electromechanical modes of the power system by influencing the significant states is revealed.

Afterwards, an equivalent coefficient model for a non-stiff grid is proposed in this project. With the derived equivalent coefficients, the relationship between the dynamic characteristics of the SSSG and the main parameters are revealed. Furthermore, by using the proposed equivalent coefficient model, the conditions to achieve dynamic active power sharing are discussed and an inertia control strategy to take care both of the local load disturbance

and the set-point variation are proposed, respectively.

The stability analysis and control of the SSSG are also addressed in this thesis. On one hand, to cope with the active power oscillation of the basic SSSG, a damping control strategy is proposed based on the acceleration control. The root locus-based small-signal stability is guaranteed by proper parameters design. On the other hand, the transient of the SSSG internal voltage is investigated quantitatively, which reveals how the internal voltage deteriorates the transient angle stability of the traditional SSSG. Then, an enhanced SSSG is proposed with better a transient angle stability.

Further, the coupling of different control loops is considered in this thesis, too. Unlike seeing the DC source as ideal and power loops being independent, a multivariable feedback control structure is proposed. All of the control targets of both DC and AC sides are taken care of simultaneously, which enables the SSSG to have superior and robust performance. An H_∞ optimization is used to tune all the parameters of the controller simultaneously.

The findings of this Ph.D. project enables a better integration of the SSSGs in the power system.

Resumé

Solid-state (baseret på effektelektronik) synkron generatoren (SSSG) er en lovende måde at integrere fremtidens generatorer (baseret på sol og vind) i el-systemet, da de er inverter-baseret og kan opføre sig som den synkrone generator (virtuel synkron generator, VSG), men har ikke en roterende masse. Ikke desto mindre er der store forskelle i modellering, kontrol og anvendelse af SSSG'en sammenlignet med synkron generatoren (SG) og dette giver nye udfordrende problemer for at sikre en stabil drift af el-systemet og dette er hoved-temaet i dette PhD projekt.

For det første medfører forskellige detaljerede matematiske modeller, der bruges i SSSG'en til at efterligne en SG, uundgåeligt forskellige egenskaber ved el-systemet og for så vidt også SSSG'en internt. Samtidig bliver selve el-systemets struktur mere distribueret og el-nettet er ofte ikke så kraftig som det normale el-system, hvilket betyder at den normale analyse-metode for SG, eksempelvis baseret på en enkelt-generator og et uendeligt stærkt el-net ikke kan ikke give en fyldestgørende evaluering af SSSG'en i el-nettet, hvorfor en mere detaljeret analyse af SSSG'en er nødvendig.

For det andet giver en effekt-elektronisk baseret SSSG mulighed for at tilføje mere fordelagtige funktioner for el-nettet, som en SG ikke har, og dermed kunne levere en forbedret og mere robust ydeevne ved hjælp af avancerede kontrol-algoritmer. For at kunne optimere SSSG's ydeevne bør koblingen mellem de flere kontrolsløjfer der eksisterer i SSSG'en også analyseres for at udnytte fordelene ved SSSG'en.

For at bidrage til ovennævnte udfordringer undersøger dette ph.d. projekt de dynamiske egenskaber ved SSSG'en og foreslår avanceret kontrol-metoder, der forbedrer SSSG'ens egenskaber sammenlignet med en traditionel SG. Forskellige modellerings metoder af SSSG'en sammenlignes med hinanden og også med den traditionelle SG. Ydermere undersøges SSSG's indvirkning på den elektromekaniske svingning, der ses i det traditionelle el-net med mange SG'er ved anvendelse af små-signal analyse, samt ved analyse af hvilke dynamiske forhold, der er de mest kritiske i det system der analyseres (participation factor).

Derefter foreslås i afhandlingen en koefficientmodel for SSSG'en, når den

er tilsluttet et svagt el-net. Med de bestemte ækvivalente koefficienter afsløres forholdet mellem SSSG's dynamiske egenskaber og nøgle parametrene i det øvrige el-net. Ved at anvende den foreslåede ækvivalente koefficientmodel diskuteres endvidere betingelserne for at kunne opnå en dynamisk deling af aktiv effekt, når flere SSSG'ere er tilsluttet. Der foreslås endvidere en kontrolstrategi, der deler inertien i de enkelte SSSG'ere for at kunne håndtere både den lokale belastningsforstyrrelse og variationen i setpunkterne til SSSG'erne.

Endvidere analyseres stabilitetskontrollen af SSSG'en også i dette projekt. Der foreslås en dæmpningsstyrings-strategi, som er baseret på en accelerationskontrol til at håndtere svingningerne i den aktive effekt for den traditionelle SSSG. Stabiliteten opnås ved en korrekt parameter design ved brug af rod-kurver og små-signal analyser. Samtidig undersøges SSSG'ens interne spænding kvantitativt og som afslører hvordan den interne spænding kan forringe den transiente vinkelstabilitet i den traditionelle SSSG. I projektet foreslås endvidere en forbedret SSSG kontrol strategi, der giver en bedre vinkelstabilitet i el-nettet.

Endelig undersøges koblingen og designet af de forskellige kontrolsløjfer, som er i SSSG'en. Normalt betragtes DC-kilden i SSSG'en som ideel og uafhængig af de strømsløjfer, der anvendes til netstyringen (AC) – I dette projekt foreslås en multivariabel tilbagekoblings –kontrolstruktur, der medtager alle tænkelige koblinger i SSSG'en. Både DC og AC siderne bliver håndteret samtidigt og som gør det muligt for SSSG'en, at opnå en meget robust ydeevne. En H_∞ optimerings-metode er brugt til at indstille alle parametrene for regulatorerne samtidigt og de frembragte resultater ser lovende ud.

De mange opnåede resultater af dette ph.d. projekt muliggør en bedre integration af SSSG'erne i fremtidens el-system og det er en meget lovende teknologi for et bæredygtigt samfund.

Contents

Preface

This Ph.D. thesis is a summary of the outcome from the project "*Modeling and Control of Solid-State Synchronous Generator*", which was carried out at AAU Energy, Aalborg University, Denmark.

First of all, I would like to extend my sincere thanks towards my supervisor Professor Frede Blaabjerg for his careful and valuable guidance during my Ph.D. study. His care and help give me great encouragement and his rigorous and diligent attitudes have been inspiring me in the past three years. I would also like to thank my co-supervisor Associate Professor Dao Zhou for his suggestion, guidance, and support during my Ph.D. study.

I would like to thank Associate Professor Florian Dörfler for providing me an opportunity to visit Swiss Federal Institute of Technology Zurich (ETH Zurich) during my study abroad and broaden my knowledge in the area of control theory. I am also grateful to my new friends at IFA-ETH Zurich for their valuable discussion about multivariable feedback control in the grid-forming converter, which is important to my Ph.D. study.

I would further like to thank all my colleagues at AAU Energy, Aalborg University for their fruitful discussion and great help for the experiments, and all the secretaries for their help during my Ph.D. study.

Last but not least, I would like to express my deepest gratitude to my family. During my Ph.D. study, they have always shown their encouragement, which is my biggest support.

Due to the corona virus, the last time of my Ph.D. study is special. Once again, I would like to thank my motherland China, my supervisors, my family, and all my friends for their help in many ways.

Meng Chen
Aalborg University, September 29, 2021

Part I

Report

Chapter 1

Introduction

1.1 Background

The modern power and energy system are facing profound changes, where the traditional energy production dominated by the fossil energy has not been able to address the environmental concerns and meet the increasing electrical power demands. In this context, more and more inverter-interfaced generators (IIGs) such as photovoltaic (PV), wind turbine, and energy storage system (ESS) are being integrated into the traditional AC power system due to their potential to diminish the need for energy originated from fossil fuels and thereby decrease the greenhouse gas emissions [1,2]. The global installed capacity of wind power (including both of onshore and offshore) is expected to be 20150 GW up to 2030, and the number is 2840 GW for PV [3, 4]. In terms of Denmark, the electricity supply capacity including wind power and PV is expected to be more than 18 GW as shown in Fig. 1.1, from which the renewable energy share in electricity consumption is expected to be 55% [5]. Nevertheless, the high penetration of IIGs will change the characteristics of the conventional centralized power system and challenge its stable operation due to low physical inertia, hardware limitations of the power semiconductor devices, poor frequency and voltage regulation abilities of the common used grid-following control of IIGs [6–10].

From the perspective of control, a grid-following IIG behaves like a controlled current source as shown in Fig. 1.2(a). The grid-following IIG can achieve quick power tracking thanks to its high bandwidth and can also provide virtual inertia with a proper control. However, the grid-following IIG still relies on the power grid usually via a phase-locked loop (PLL), which makes it suitable to connect into a strong grid. To free this requirement, a grid-forming IIG as shown in Fig. 1.2(b) has been proposed to operate without relying on a strong grid. Unlike a grid-following IIG, the grid-forming

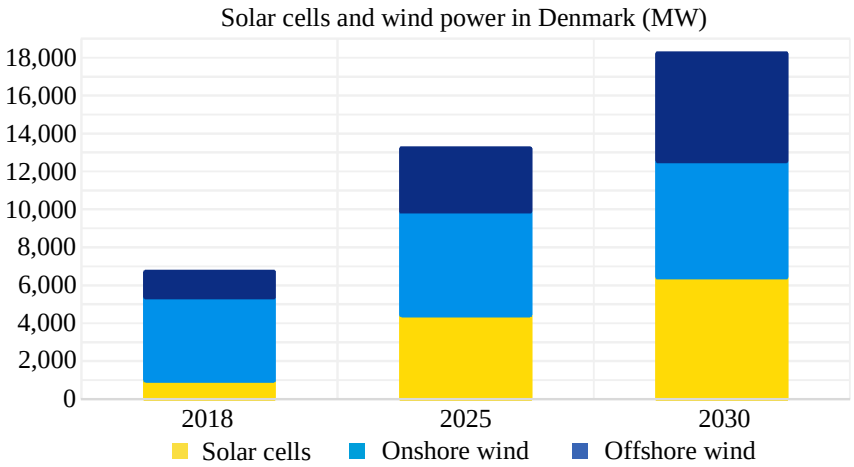

Fig. 1.1: Electricity supply capacity of PV and wind in Denmark. Source: [5]

IIG behaves as a controlled voltage source, which makes it suitable to connect into a weak or even operate in islanded grid [1].

In the past, the power system has been dominated by synchronous generators (SGs) with suitable control of the governor and automatic voltage regulator (AVR). The mechanical rotor of the SG provides a large inertia to restrain the frequency nadir and the rate of change of frequency (RoCoF) during various disturbances. The governor and AVR enable the SGs to actively participate in the frequency and voltage regulation, and achieve automatically power sharing in a decentralized way. Meanwhile, the SG can provide a high short-circuit current several times (e.g., 5-10 times) of its rated value, which make it easy to establish a protection system in the power system. These features have been proven to be favorable for the stability of the power system. Motivated from the SG behavior, one of the potential methods to cope a the high penetration of IIGs is to let the outputs of IIGs emulate the terminal characteristics of the SG regardless of the differences in the fundamental hardware [11, 12]. As an IIG has no rotating components and it is not an real SG, an IIG with features like the SG can be called (referring to the so-called solid-state transformer [13]) solid-state SG (SSSG), or virtual SG (VSG) [14–16]. Similar concept are also known as synchronverter [17, 18], virtual synchronous machine [19, 20], etc. In the context that more (SGs) are replaced by the IIGs, the grid-forming ability is necessary for the IIGs in order to keep the stability of both frequency and voltage. Therefore, this Ph.D. project mainly focuses on the grid-forming SSSG.

Table 1.1 summarizes and compares some key features of the SG and the SSSG. To mimic the terminal characteristics of the SG, an SSSG relies on proper control algorithms and hardware implementations. On one hand,

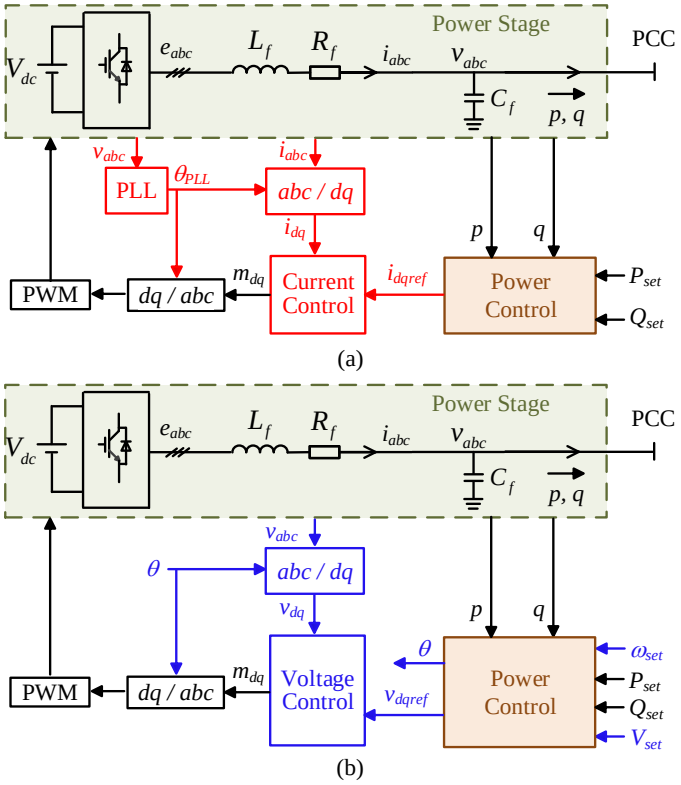

Fig. 1.2: General topology and control block diagram of IIG. (a) Grid-following control. (b) Grid-forming control.

the control should well replicate the inertia characteristics of the rotor and the regulation characteristics of the governor and AVR. On the other hand, the DC source of the SSSG should provide enough energy to successfully behave like the short-term inertia response and long-term regulation ability. Meanwhile, the hardware limitations of the SSSG restrain its short-circuit capability compared with the SG even though the control system can emulate the SG. Nevertheless, the SSSG has also superiority over the SG. The model of the SG is highly determined by its physical components, whereas the SSSG is mainly control dominated [21]. Therefore, besides the necessary features, an SSSG may avoid to introduce the complicated model of the SG, governor, and AVR. From the perspective of this point, it is also possible to add more favorable features for the grid operation, where an SG cannot do, into the SSSG motivated by its good controllability. Overall, a grid-forming SSSG is a promising solution to solve the problems of the replacement of the SGs by the IIGs, and it is expected to have many applications in the future power system. To achieve this, there are several issues in both control and hard-

Table 1.1: Comparisons between synchronous generator (SG) and solid-state SG

Features		SG	SSSG
Inertia	Energy	Kinetic energy in rotor	DC source (e.g., DC-link capacitor, ESS, reserves of renewable energy)
	Realization	Physical rotor	Control algorithm
Regulation	Energy	Prime motor	DC source
	Realization	Governor and AVR	Control algorithm
Short-circuit capability		High	Low
Modeling		Physical dynamics	Control algorithm
Controllability		Low	High

ware implementation of the SSSG, which need to be investigated. This Ph.D. project focuses mainly on the control of SSSG, while the limitations and improvement in the hardware in order to obtain a "real" SSSG is not discussed in details.

Fig. 1.3 shows an analogous diagram between the SG and SSSG. The power stage of the SSSG consists of a DC source, a three-phase inverter, and an LC filter connected to the point of common coupling (PCC). To mimic the actual governor and AVR of the SG, the SSSG uses a virtual governor and a virtual AVR to regulate the frequency and voltage. Meanwhile, a virtual rotor and a virtual winding are used to emulate the electromechanical and electromagnetic characteristics of the SG, respectively. In this way, the SSSG can exchange power with the external power grid in a similar way as an SG, where, from the view point of the external power grid, the SSSG is equivalent to an SG to some extent when neglecting the high-frequency switching process by using state-space averaging. The studies on the SSSG in this Ph.D. thesis are all based on the basic structure shown in Fig. 1.3(b).

Although the basic principle and key feature (i.e., virtual inertia represented by H as shown in Fig. 1.3(b)) is similar, there may be different ways to realize an SSSG [14]. As the aforementioned discussion, unlike the SG whose model is restricted by the physical entity, the SSSG is mainly control-based. Thus, some simplified models may be preferred in order to both make the SSSG operation simple and not to introduce unexpected terminal characteristics. As a result, the analysis of the SGs based on a high-order model may not apply to the SSSGs. Actually, corresponding to each component of the SSSG, various models have been used [22]. Therefore, the performance of the SSSG and thereby its impact on the power system will be different compared to an actual SG in some cases. Meanwhile, the voltage and current control

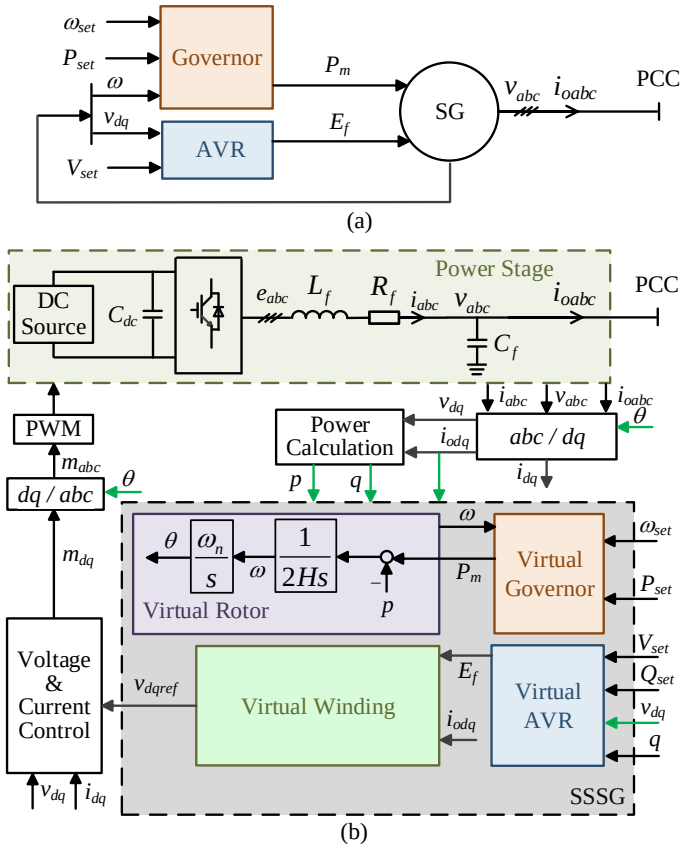

Fig. 1.3: Analogous diagram between SG and SSSG. (a) SG. (b) SSSG. ω_{set}, P_{set}, V_{set}, and Q_{set} are the set-point values of angular frequency, active power, terminal voltage, and reactive power. ω_n is the nominal angular frequency. ω is the angular frequency from the (virtual) rotor. P_m is mechanical power from the (virtual) governor. E_f is the internal voltage from the (virtual) AVR. e_{abc} are the output voltages of the inverter. v_{abc} are the terminal voltages. q is the output reactive power. H is the inertia constant. Source: [J5].

loops will also influence the behavior of the SSSG.

Not only the generators themselves, but also the structure of the power system is changing as more IIGs are integrated. Unlike the traditional hierarchical structure, where the SGs are usually connected into the transmission system and far away from the load center, the future power system may be more distributed, where the distributed generators (DGs) account for a larger and larger percentage of the generation capacity [23]. Moreover, new grid structures such as microgrid may also play an important role in the future power system due to its benefits on integrating, managing and optimizing the DGs. Compared with the SGs, the aforementioned changes of the power system will influence the characteristics of the SSSGs in those applica-

tions [24]. On one hand, the SSSGs may be located closer to the loads, where the load disturbances may have significant impact on the performance of the SSSGs. On the other hand, the PCCs where the SSSGs are connected may not be very stiff. E.g., microgrids are expected to operate in the islanded mode when necessary, where, in this context, several SSSGs may be paralleled with each other in a decentralized way to support the voltage and frequency, and no dominant units will exist [24]. Obviously, the characteristics of the SSSG in these cases may be quite different from connecting to an ideal infinite bus, which should be further investigated.

The basic SSSG can emulate the inertia characteristics, frequency and voltage regulation abilities of the SG. Nevertheless, stability issues such as small-signal stability and transient stability may still occur in the future power system with SSSGs [25,26]. Although many related researches have been reported for the SG dominated system, it has been pointed out that the SSSGs are different from the SGs due to distinctions in both modeling and applications. Meanwhile, from the aforementioned discussion, it is possible for the SSSG to provide better and robust performance responding to different disturbances by using proper control strategies due to the fact that the SSSG is mainly control-dominated. Motivated by this, the advanced control to achieve more control targets beyond the basic SSSG is of high interest [26]. Moreover, as an interface of power conversion, the dynamics between the DC-link capacitor of the SSSG and the AC grid are inevitably coupled with each other, which is a singular problem and does not exist in an actual SG. A good control strategy should take care of both the DC and AC sides in order to optimize the performance of the SSSG. In conclusion, more analysis and control of the SSSG are of key importance in order to develop a more stable and robust power system using SSSGs.

1.1.1 Modeling of Solid-State SG

As shown in Fig. 1.3(b), the SSSG should be able to emulate the characteristics of the SG by four parts, i.e., the virtual windings, virtual rotor, virtual governor, and virtual AVR, where all of them can have different dynamics and models. The model of the windings represents the electromagnetic characteristics, which can be classified into different orders based on various simplifications. Fig. 1.4 summarizes these representations of both the SGs and SSSGs, where the 2nd-order [17, 27–29], 4th-order [30], and 7th-order [19,31–33] models have been used for the SSSG. The virtual rotor represents the electromechanical characteristics, which is the most important part of the SSSG due to the inertia and damping. The different models of the virtual rotor mainly come from the different damping terms. As there is no real rotor, the rotor speed variation for damping in the SSSG may be expressed as the error between the virtual rotor speed and the grid frequency obtained

from a PLL [27]. To avoid the use of PLL, the grid frequency can be replaced with a constant set-point frequency [17], which makes the damping to be identical with the droop characteristics of the governor. As shown in Fig. 1.3(b), this Ph.D. thesis also avoids to use the PLL. In terms of virtual governor and virtual AVR, they enable the SSSG to participate in the frequency and voltage regulation using droop characteristics like implementation in the actual governor and AVR. However, whether the time constant of the physical parts should be emulated leads to different models of the SSSG [30, 34]. Meanwhile, various feedback signals such as the reactive power and capacitor voltage may be used to establish the droop characteristics, which enriches the categories of the virtual AVR as well [35].

Obviously, the SSSGs using various models will behave different dynamics, which leads to three main issues. First, due to the distinctions in modeling, the SSSG may not ideally emulate an SG. Especially, the most popular 2nd-order simplified model cannot reflect any transient and sub-transient behavior of the SG. The differences between the SSSG and SG have been observed and studied by some simulation analysis [34]. Second, the dynamics among different SSSGs are not identical as well. It has been proved that the SSSGs with various virtual windings or rotors may behave quite different in terms of stability performance [35, 36]. And an interesting thing is that the SSSG with a high order model may introduce unfavorable features, e.g., synchronous oscillations [35]. Besides, the voltage and current control loops also have great influence, especially with a large filter inductance [37]. Third, when the SGs are replaced by the SSSGs, their different features will change the dynamics of the power system [38], where an important example is the electromechanical oscillation. As the SSSGs are controlled by the swing equation, a similar problem of electromechanical oscillations like in the SGs may occur. Nevertheless, it is shown that the SSSG using a 2nd-order model has a potential ability to damp these oscillations [39]. However, in some cases, the opposite impact can be observed as well [40, 41].

Although, as described above, several studies have concluded in respect to different modelings of the SSSG, it is still an important topic to be investigated. The dynamics of the SSSG and SG under various disturbances need to be further compared. Moreover, a comprehensive discussion on the modeling of the virtual AVR is missing. Furthermore, the mechanism of the SSSG influencing the electromechanical oscillation of the power system is still not clear.

1.1.2 Characteristics Analysis of Solid-State SG

When connected into the power system, the characteristics of the SSSG will be influenced by both itself and the external system, which should be investigated in order to better understand the future power system with SSSGs

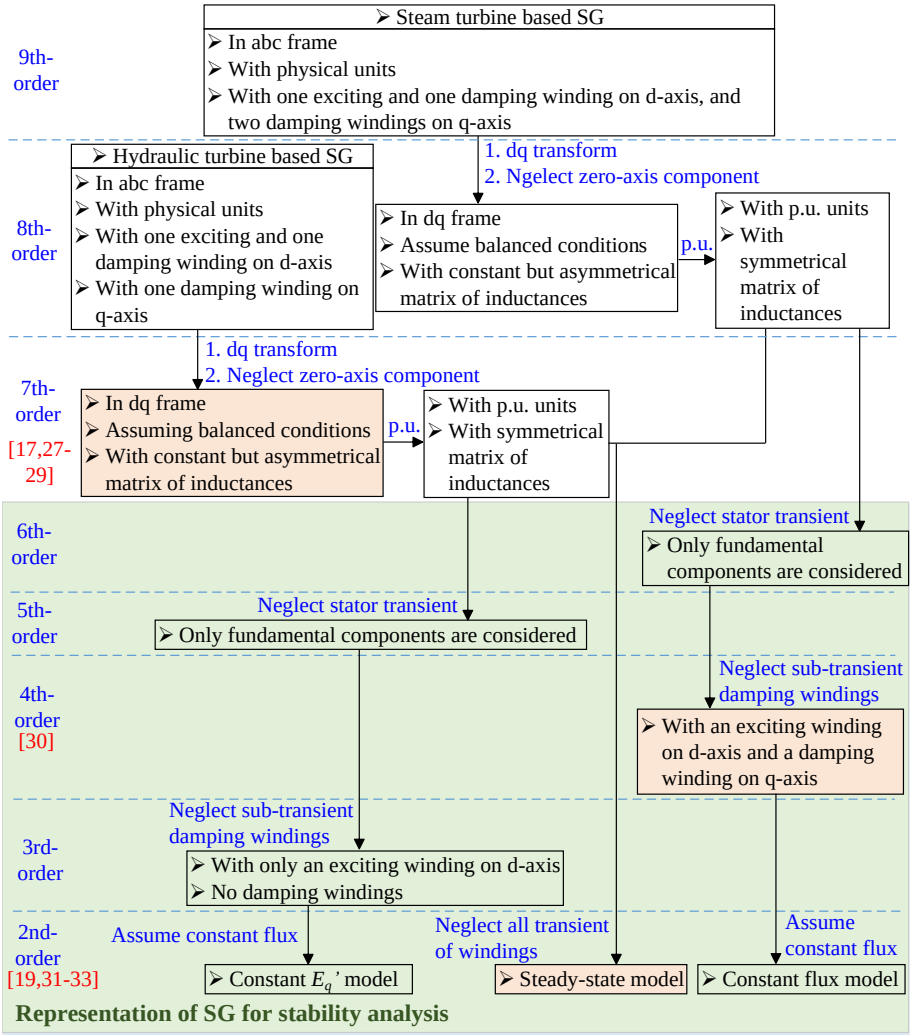

Fig. 1.4: Summary of different representation orders for SG and SSSG, where representation in orange blocks has been used to model SSSG. Source: [J1].

and guide the parameters adjustment. These influences have been studied from different aspects such as robust stability [42], frequency-domain characteristics [43], and transient active power circulation [44]. Nevertheless, some traditional indices such as RoCoF, the frequency nadir, etc., are preferred from the perspective of frequency stability, which are highly determined by the characteristics of inertia, damping, etc.

In the traditional SG, the Phillips-Heffron model is widely used to analyze the inertia and damping characteristics as shown in Fig. 1.5 [45]. In

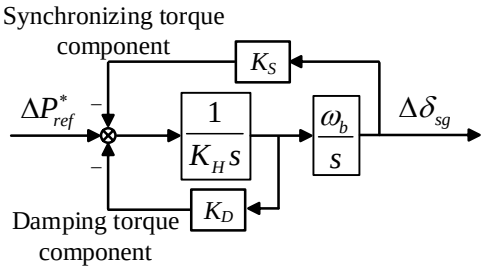

Fig. 1.5: Phillips-Heffron model used in analysis of traditional SG. Source: [J3].

this model, the characteristics of the SG are divided into three parts, i.e., the inertia characteristics represented by the equivalent inertia coefficient K_H, the damping characteristics represented by the equivalent damping coefficient K_D, and the synchronizing characteristics represented by the equivalent synchronizing coefficient K_S. To obtain these equivalent coefficients, a simulation-based method can be used [46]. A better approach is based on a small-signal analysis, which can derive the direct relationship between the equivalent coefficients and the parameters of the studied system. The equivalent coefficients have been proved as being effective in the analysis of a PLL-based doubly-fed induction generator based (DFIG-based) wind turbine system [47] and also in a photovoltaic (PV) system [48]. Similar analysis can be applied to the grid-forming controllers without PLL such as the droop control [49] and SSSG [50]. Although the studies are limited, it has been revealed how the equivalent coefficients and then the characteristics of the SSSG are influenced by both the control and system parameters in a single-machine-infinite-bus (SMIB) system [50].

However, the SMIB system cannot represent all of the possible operation conditions of the SSSGs in the future power system due to the more distributed nature in the power system. In this context, the characteristics of the SSSG are still not clear.

1.1.3 Advanced Control of Solid-State SG

The power stage of the SSSG is based on a power electronics inverter, which has a high controllability. This is the reason that the basic SSSG can easily mimic important features such as inertia by embedding the models of SGs in the control system. However, by only emulating the basic SG, some stability problems in the traditional SG-based power system still exist in a system with SSSGs.

One of the most important stability problems in the traditional power system is the angle stability related to the rotor of the SGs. Obviously, it will also be introduced in the power system by the virtual rotor of the SSSG.

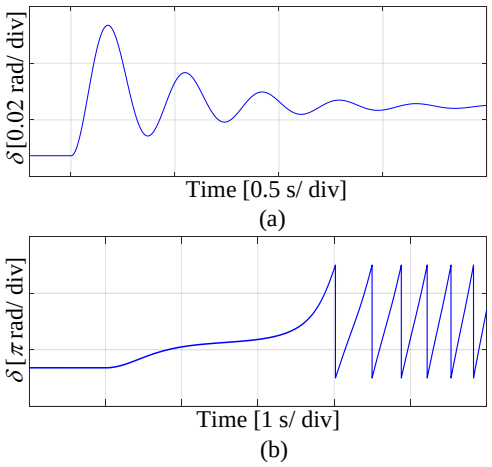

Fig. 1.6: Stability problems in SSSG. (a) Large angle oscillation responding to load disturbance. (b) Transient angle instability responding to voltage sag. Source: [J2] and [J4].

Generally, the rotor stability can be classified into small-signal stability and transient stability [51]. With a poor small-signal stability, large power and angle oscillations will occur, especially in a paralleled system, due to the dominant conjugate plural eigenvalues with small damping ratios [52]. With poor transient angle stability, the system variables will deviate from the potential equilibrium during the grid fault due to the power angle going across its critical value. These phenomena are also observed in the SSSG, as illustrated in Fig. 1.6. Therefore, in order to better take the advantages of the controllability of the inverter, improved SSSGs with superior and robust performance are expected to be proposed based on the basic SSSG in order to provide more favorable features [53].

To decrease the oscillations of the SSSG, the PLL-based or droop-based damping terms are common choices, which are effective when connected into a stiff grid [54, 55]. Besides, several PLL-free methods are also proposed in order to eliminate the potential instability of using a PLL [56–58]. Another class of damping control is based on the online adjustment rather than fixed parameters [28, 59–61]. The aforementioned methods are mainly studied focusing on a single SSSG system. With respect to a paralleled SSSGs system, the small-signal stability can be improved by a central controller due to the application of the communication technology in the power system. In this context, the center of inertia is possible to be derived, which can be used to damp the oscillations [62]. Nevertheless, the decentralized controllers using only local information are more preferred due to high reliability and flexibility, where the virtual impedance may be used. It has been proved that the power oscillations can be well damped if a specific parameter relationship of the SSSGs are met, although it is hardly guaranteed in practice [24, 52].

Furthermore, a high-pass filter based damping term can be used to decrease but will not fully eliminate the power oscillations when the parameters are mismatched [52]. Therefore, proper damping control is still required to deal with the mismatch of parameters between paralleled SSSGs.

Compared with the small-signal stability, the transient angle stability control of the SSSG is limited due to the difficulties in analyzing the non-linear characteristics. Nevertheless, some simple analysis have highlighted different transient characteristics between SSSG and SG [26,63]. Especially, it has been shown by qualitative analysis that the virtual AVR may deteriorate the transient angle stability of the SSSG [26]. However, a detailed quantitative analysis is still missing. In order to improve the transient angle stability, some control strategies are proposed as well. Like in the small-signal control, the center of inertia based on the communication can still be used [64]. In the decentralized structure, a PLL-based frequency signal has been proved to be effective when adding in either the virtual governor or the virtual AVR [63,65,66]. Similarly, the voltage signal can be used by the virtual governor to improve the transient angle stability [26]. In addition, other more complicated control strategies such as mode-adaptive control [67], non-linear back-stepping design [68], etc., are also proposed. Nevertheless, the aforementioned methods will compromise simplicity, steady-state regulation, PLL-free operation, and decentralization.

Another problem comes from the coupling between the DC and AC sides in the inverter, which is rarely considered. As a result, the performance of the SSSG can be limited, too. Therefore, new advanced control strategies of SSSG, which can take care both of the dynamics of DC and AC sides, need to be explored in more details.

1.2 Project Objectives and Limitations

1.2.1 Project Objectives

Motivated by the gaps of the existing research and the trend of many more IIGs in the grid discussed above, this Ph.D. project focuses on the main question of:

"How to enable a stable and grid-friendly integration of the IIGs by controlling them as SSSGs?"

That gives the following sub-questions as follows:

- What are the distinctions and impact of the SSSGs using different modelings in the power system?
- How will the parameters influence the characteristics of the SSSGs when integrated into a non-stiff grid?

- How to provide a superior and robust performance of the SSSG responding to different disturbances by advancing its control system?
- How to simultaneously take care of the AC and DC dynamics in the control design of the SSSG in order to improve and optimize the performance using modern control theory?

Base on this, to solve the questions, the following objectives of this Ph.D. project are defined:

- **Compare and analyze the performance of different SSSG modeling methods**

  Various modeling of the virtual winding and the virtual AVR need to be compared with each other and with the SG in this Ph.D. project. Thereafter, the impact of the simplified 2nd-order SSSG on the electromechanical oscillation need to be investigated in order to propose a damping strategy for the electromechanical oscillation by using SSSGs.

- **Analyze the characteristics of the SSSG when integrated into the non-stiff grid**

  An equivalent coefficient model need to be developed in order to reveal the impact of the parameters on the characteristics of the SSSGs in a non-stiff grid. By using the equivalent coefficient model, the conditions of the dynamic active power sharing and a modified inertia control need to be proposed, respectively, in order to achieve a better dynamics responding to different disturbances, e.g., load step and set-point value changing.

- **Develop improved control strategies of the SSSG and analyze the stability**

  Focusing on the small-signal disturbance, an improved damping control need to be explored and added in the basic SSSG in order to suppress the power oscillations due to the parameters mismatch. Besides, focusing on the large-signal disturbance, a control strategy to enhance the transient angle stability should be proposed as well. Furthermore, the small-signal and large-signal analysis need to be carried out in order to help the parameters design and to evaluate the proposed methods.

- **Develop the multivariable feedback control of the SSSG by considering the AC/DC coupling**

  A generalized multi-input-multi-output (MIMO) configuration with considering the AC/DC coupling will be developed to unify the SSSG and some other grid-forming controllers, which will reveal their essences

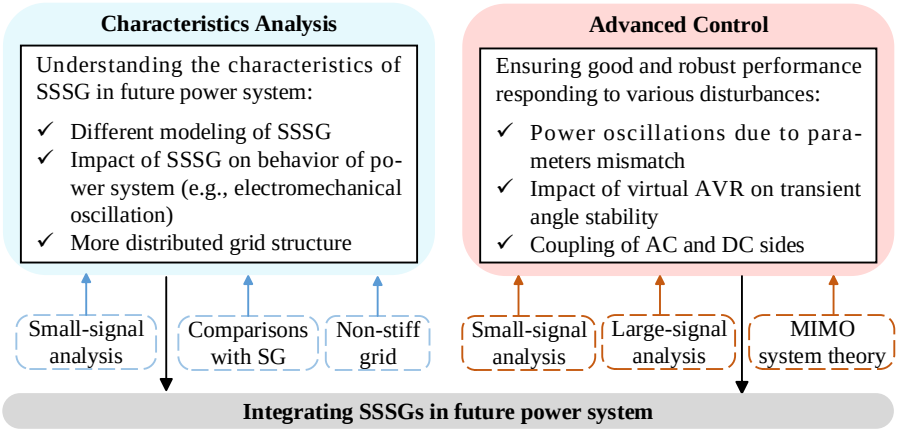

Fig. 1.7: Research activities in the Ph.D. project: Modeling and Control of Solid-State Synchronous Generator.

from the view of the control theory. Thereafter, a multivariable feedback control will be designed in order to optimize the performance of the SSSG.

An overview of the research activities of the Ph.D. project are graphically shown in Fig. 1.7.

1.2.2 Project Limitations

This Ph.D. project mainly focuses on the power loops control of the SSSG, whereas the dynamics of the inner loops are neglected and the hardware limitations are not considered in details. Actually, the inner loops may also influence the stability of the SSSG especially in the case of low switching frequency. However, it is supposed that the parameters of the inner loops have been well designed to decouple the dynamics of the inner loops and the power loops.

In the analysis and design of the SSSG, symmetric three-phase systems are used, which means various unbalanced cases (e.g., single-phase load, unbalanced fault, etc.) are not investigated. Also, this Ph.D. project only focuses on the fundamental frequency, whereas the high-frequency switching of the inverter is neglected. Furthermore, no harmonic sources such as nonlinear loads are considered.

In order to achieve the functions of the SSSG, a certain amount of reserve energy is necessary, where various energy storage systems may be used in practical applications. However, in this Ph.D. project, the DC source is simplified to be ideal when not using the DC dynamics due to the decoupling feature of the PWM. When considering the coupling between AC and DC

sides in the multivariables feedback control structure, the DC source is still simplified to be a controlled current source. The aforementioned assumptions indicate that there are always enough energy in the DC source. Otherwise, the functions of the SSSG may not be performed.

1.3 Thesis Outline

The outcome of the Ph.D. project is summarized in this Ph.D. thesis on the basis of the collection of the published papers. The thesis consists of two main parts: ***Report*** and ***Selected Publications***. Fig. 1.8 presents the structure of this Ph.D. thesis, where the corresponding selected publications of each chapter are indicated as well.

In *Chapter* 1, an introduction about the background, motivation, and objectives of this Ph.D. thesis is given. The following two chapters study the characteristics of the SSSG, where *Chapter* 2 compares different models of the SSSG and the impact on the electromechanical oscillation from the the source-side view, and *Chapter* 3 is from the view of the grid-side and discusses the characteristics of the SSSG in the non-stiff grid using a equivalent coefficient model. Afterwards, *Chapter* 4 and *Chapter* 5 deal with the advanced control of the SSSG to provide a superior and robust performance. Specifically, *Chapter* 4 focuses on the angle stability from both aspects of the small-signal and large-signal, while in *Chapter* 5, a new MIMO control configuration of the SSSG is proposed and designed, which is able simultaneously to consider the dynamics of the AC and DC sides and also to optimize the performance. Finally, the main contributions and future work are concluded in *Chapter* 6.

1.4 List of Publications

The results and outcomes during the Ph.D. study are included in several publications as listed in the following, which are selected in this Ph.D. thesis as shown in Fig. 1.8.

Journal Papers

J1. **M. Chen**, D. Zhou, and F. Blaabjerg, "Modelling, implementation, and assessment of virtual synchronous generator in power systems," *J. Mod. Power Syst. Clean Energy*, vol. 8, no. 3, pp. 399-411, May 2020.

J2. **M. Chen**, D. Zhou, and F. Blaabjerg, "Active power oscillation damping based on acceleration control in paralleled virtual synchronous generators system," *IEEE Trans. Power Electron.*, vol. 36, no. 8, pp. 9501-9510, Aug. 2021.

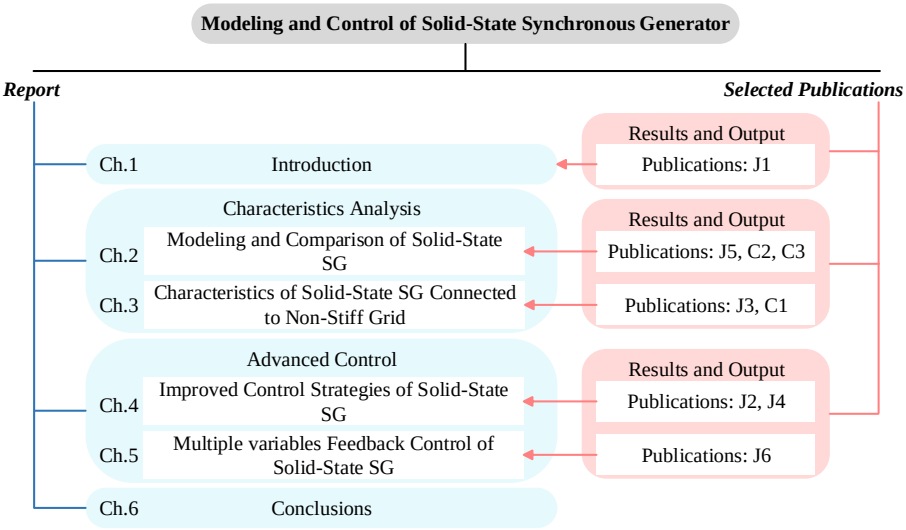

Fig. 1.8: Structure and corresponding selected publications of Ph.D. thesis.

J3. **M. Chen**, D. Zhou, C. Wu, and F. Blaabjerg, "Characteristics of parallel inverters applying virtual synchronous generator control," *IEEE Trans. Smart Grid*, doi: 10.1109/TSG.2021.3102994, Status: Early Access.

J4. **M. Chen**, D. Zhou, and F. Blaabjerg, "Enhanced transient angle stability control of grid-forming converter based on virtual synchronous generator," *IEEE Trans. Ind. Electron.*, doi: 10.1109/TIE.2021.3114723, Status: Accepted.

J5. **M. Chen**, D. Zhou, and F. Blaabjerg, "High penetration of inverter-based power sources with VSG control impact on electromechanical oscillation of power system," *IEEE Trans. Power Deliv.*, Status: Under Review.

J6. **M. Chen**, D. Zhou, A. Tayyebi, E. Prieto-Araujo, F. Dörfler, and F. Blaabjerg, "Generalized multivariable grid-forming control design for power converters," *IEEE Trans. Smart Grid*, Status: Under Review.

Conference Papers

C1. **M. Chen**, D. Zhou, and F. Blaabjerg, "Characteristics of virtual synchronous generator based voltage source converter," in *2020 IEEE Power Energy Soc. Gen. Meet. (PESGM)*, Montreal, QC, Canada, 2020, pp. 1-5.

C2. **M. Chen**, D. Zhou, and F. Blaabjerg, "Impact of synchronous generator replacement with VSG on power system stability," in *2020 IEEE 21st*

Work. Control Model. Power Electron. (COMPEL), Aalborg, Denmark, 2020, pp. 1-7.

C3. **M. Chen**, D. Zhou, and F. Blaabjerg, "Voltage control impact on performance of virtual synchronous generator," in *2021 IEEE 12th Energy Convers. Congr. Expo. - Asia (ECCE-Asia)*, Singapore, Singapore, 2021, pp. 1981-1986.

- **M. Chen**, D. Zhou, and F. Blaabjerg, "A decentralized adaptive SOC balancing strategy in VSG-based islanded power system," in *2021 47th Annual Conference of the IEEE Industrial Electronics Society (IECON)*, Toronto, Canada, 2021, Status: Accepted.

1.5 Experimental Setup Used in Ph.D. Thesis

The experimental results used in this Ph.D. thesis are all obtained based on the setup shown in Fig. 1.9. A Yaskawa D1000 regenerative converter is used to provide the DC voltage for a Danfoss drive system (i.e., inverter), which is then connected to the system via a LCL filter. A dSPACE system is used to execute the close-loop control, where the electrical signals are measured by a DS2004 A/D board and sent to a DS1007 Platform for control algorithm implementation, and a DS5101 digital waveform output board is used for PWM generation. The output waveform are shown by either a oscilloscope via a DS2101 D/A board or a personal computer (PC). The states of the breakers B1 and B2 determine the studied cases. When B1 is open while B2 closed, the studied case is a grid-connected SSSG system (used in Chapter 2, 4, and 5), where a Chroma 61845 grid simulator is used to provide the required grid voltages. When B1 is closed while B2 open, the studied system is an islanded paralelled SSSGs system (used in Chapter 3 and 4) supplying pure resistive loads. The detailed parameters will be listed in the respective chapter.

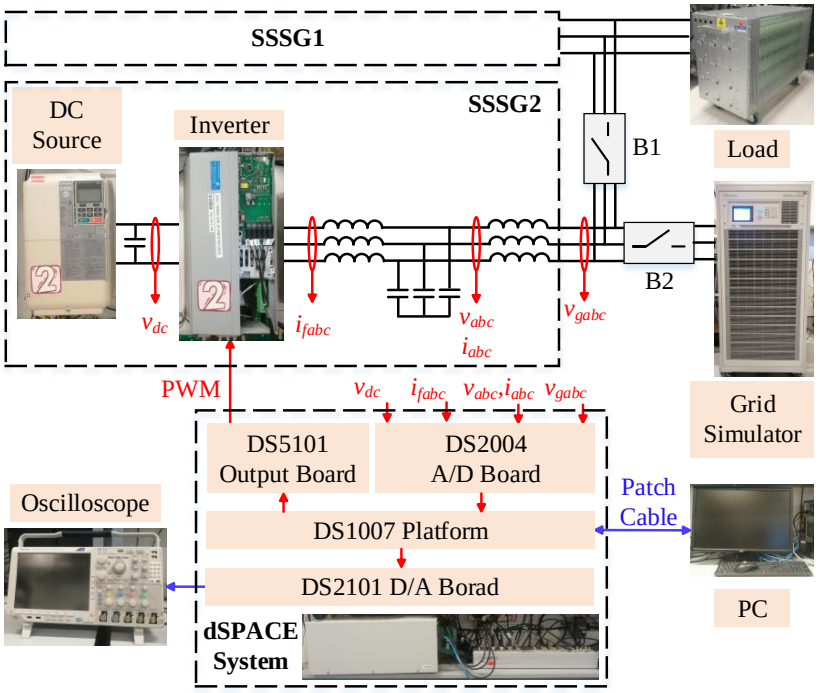

Fig. 1.9: Experimental setup used in this Ph.D. thesis. Source: [J4].

Chapter 2

Modeling and Comparison of Solid-State SG

2.1 Background

As shown in Fig. 1.3(b), an SSSG emulates an SG by a virtual rotor, a virtual governor, a virtual winding, and a virtual AVR. In the previous studies in [36] and [39], several models of the virtual rotor and virtual governor have been compared. However, the virtual windind and virtual AVR are of limited investigation.

The diversity of the SG models in terms of the windings has been summarized in Fig. 1.4, which can be from 2nd-order to 9th-order. With respect to the SSSG, the low-order models (e.g., 2nd-order or even without the virtual winding) with simple droop controls are widely used due to the simplicity. In order to mimic an SG closer, a higher-order model should be used. Nevertheless, for the stability analysis, a high-order model (e.g., over 6th-order) is rarely used even in the traditional power system. Therefore, it is of interest to compare both of steady-state and dynamic characteristics among a 2nd-order model based SSSG, a 6th-order model based SSSG, and an actual SG. It is expected that the dynamics of a power system with SSSGs will change compared to the traditional power system with only SGs (e.g., electromechanical oscillations) [38, 69, 70].

Moreover, the virtual AVR of the SSSG has also different kinds of implementation due to the flexibility of the feedback signals (e.g., terminal voltage and reactive power) [35, 36, 71]. In addition, whether the virtual winding and inner loops exist may have a significant impact on the performance of the virtual AVR. As shown in Fig. 1.3(b), E_f will be directly used to generate e_{abc} if there is no virtual winding and inner voltage and current control loops,

Table 2.1: Case Studies with Various Amounts of SSSG in IEEE 9-Bus System (Source: [C2])

Case	G1	G2	G3	Penetration	Case	G1	G2	G3	Penetration
1	SG	SG	SG	0%	3	SSSG	SSSG	SG	77.4%
2	SSSG	SG	SG	43.6%	4	SSSG	SSSG	SSSG	100%

while E_f can also be used to control v_{abc} if there is an inner loop [67].

To cope with the aforementioned issues, this chapter begins with a simulation comparison among the 6th-order, 2nd-order SSSGs, and the SG with various operation conditions using the IEEE 9-bus test system. The characteristics of the voltage regulation (related to the virtual AVR) and electromechanical oscillation are specially focused on. Then, a simple grid-connected SSSG system is used in order to theoretically evaluate various virtual AVRs and give the basis of the following study. Thereafter, this chapter investigates the mechanism of how the SSSG will influence the electromechanical oscillations of the power system by small-signal analysis using the same IEEE 9-bus test system.

2.2 Modeling and Comparison of Virtual Windings

A 6th-order model of the virtual windings includes most of the important transient and sub-transient characteristics in the stability analysis of a conventional SG. Therefore, in [C2], it is used to illustrate how close an SSSG can emulate the SG, and whether a higher-order model should be used. Thereafter, the widely used simplified 2nd-order model is also used to present what will happen if a simple model is preferred and only the key characteristics of the SG (e.g., the inertia) are emulated. The used IEEE 9-bus test system [72] is shown in Fig. 2.1 by considering four cases as shown in Table 2.1. The general structures including the control system of both SG and SSSG have been shown in Fig. 1.3. In the simulation, the standard p.u. synchronous machine model in Matlab/Simulink is used to represent the SG, where the WSCC Type G governor model and IEEE Type 1 excitation model are used for the governor and AVR, respectively [73].

A block diagram of the virtual winding in a 6th-order model based SSSG is shown in Fig. 2.2, where the virtual governor and virtual AVR are also based on the WSCC Type G governor model and IEEE Type 1 excitation model for a closer emulation, respectively . Besides, a block diagram of the virtual winding in the 2nd-order model based SSSG is shown in Fig. 2.3. With this model, the following basic droop controls are usually used to model the

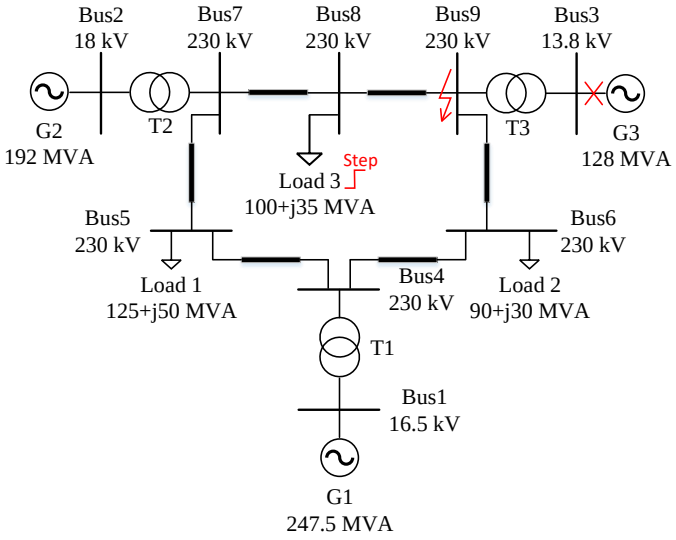

Fig. 2.1: Single-line diagram of the IEEE 9-bus system. Source: [C2].

virtual governor and virtual AVR:

$$P_m = P_{set} - \frac{1}{D_p}(\omega - \omega_{set}) \tag{2.1}$$

$$E_f = \frac{1}{T_f s + 1}[V_{set} + D_q(Q_{set} - q)] \tag{2.2}$$

where D_p and D_q are the droop coefficients, T_f is the time constant of filter.

The following four operation conditions are compared [C2]:

- **Steady-State:** Steady-state voltages of the load buses are compared.
- **Load Step:** A load step of 45 MW+j15 MVar at Bus 8 is added.
- **Three-Phase Fault:** A three-phase fault near Bus 9 is applied, which is then cleared after 3 cycles by open the breakers of the line between Bus 8 and Bus 9.
- **Loss of Generator:** G3 is disconnected from the system.

As examples, Fig. 2.4 and Fig. 2.5 show comparisons of the steady-state and response to the load step. It can be seen that, in general, the 6th-order model based SSSG will have quite similar dynamics with the SGs except small distinctions, while the 2nd-order model will behave with different characteristics. Furthermore, two issues are worthy being noticed. First, from the steady-state voltages, the 2nd-order model based SSSG may lead to severe

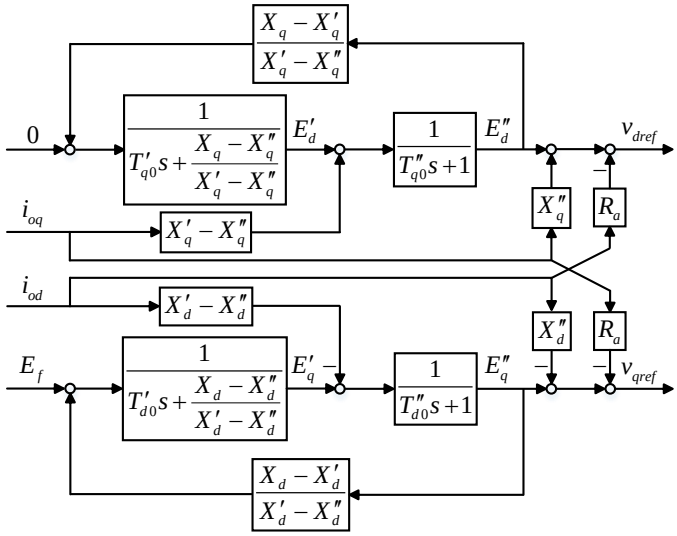

Fig. 2.2: Block diagram of virtual winding of 6th-order model based SSSG in Fig. 1.3(b). X_d and X_q are the d- and q-axis virtual synchronous reactances. Source: [C2].

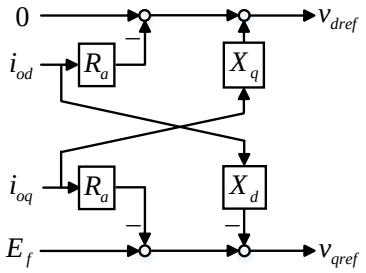

Fig. 2.3: Block diagram of virtual winding of 2nd-order model based SSSG in Fig. 1.3(b). Source: [C2].

voltage decrease, which is due to large X_{dq} and the type of virtual AVR. In Case 4 the system is even not stable at all. Second, it is observed that Case 3 has better dynamics with smaller oscillations responding to disturbances than in Case 1, which implies that the 2nd-order model based SSSG may provide favorable features in the damping. Therefore, the remaining part of this Ph.D. project mainly focuses on the 2nd-order model based SSSG. And it will be shown that the problem of voltage decrease can be improved by a suitable virtual AVR.

The following two sections will further investigate the virtual AVR and damping using the 2nd-order model based SSSG.

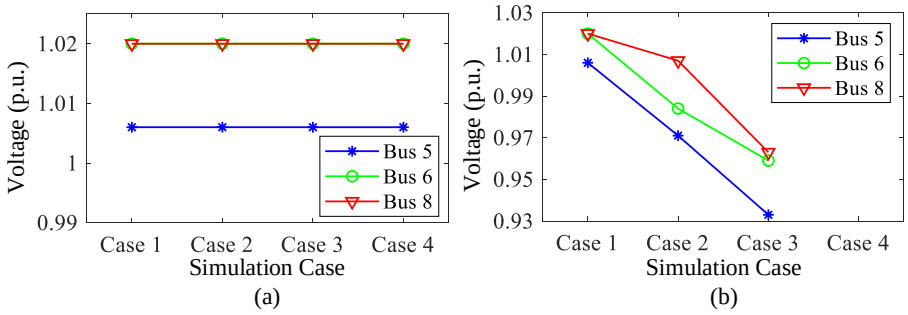

Fig. 2.4: Steady-state voltage of load buses in different cases. (a) 6th-order. (b) 2nd-order. Source: [C2].

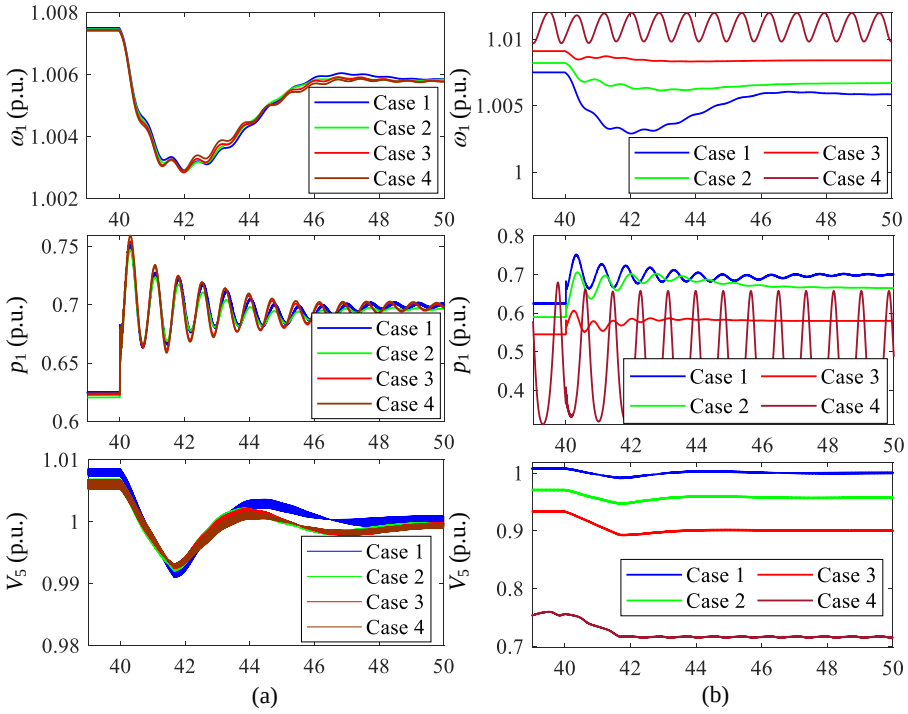

Fig. 2.5: Dynamics responding to load step of 45 MW+j15 MVar at Bus 8. (a) 6th-order model. (b) 2nd-order model. Source: [C2].

2.3 Modeling and Comparison of Virtual AVR

As the aforementioned discussion, the 2nd-order model based SSSG with a virtual AVR of (2.2) may lead to large voltage drops in the steady-state and even to instability. These observations show the important impact of

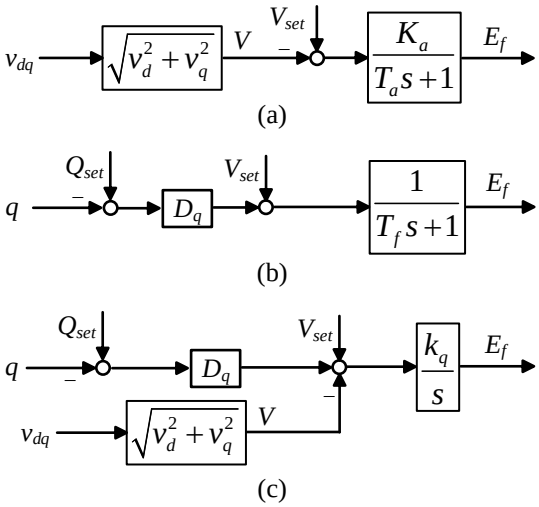

Fig. 2.6: Block diagram of three kinds of virtual AVR. (a) V-droop control. (b) q-droop control. (c) droop-I control. K_a and T_a are the gain and time constant in V-droop control. k_q is the integral gain in droop-I control. Source: [C3].

the virtual AVR. Generally, there are three kinds of often used virtual AVRs as shown in Fig. 2.6. The V-droop control is a simplification of a traditional AVR, which usually takes V as the feedback. In comparison, both of the other two virtual AVRs need the feedback of q. Although all of them can achieve a droop characteristics, their dynamics may be quite different, which are investigated and compared in [C3]. For the simplicity of theoretical analysis, a grid-connected SSSG system is used (see Fig. 1.9). As mentioned before, the simplest SSSG may not have parts of virtual winding and inner loop. Therefore, a basic SSSG is initially used. Afterwards, the impact of the virtual winding and inner loop will be taken into consideration.

2.3.1 Basic Solid-State SG

When there is no virtual winding and inner loop, E_f is directly used to generate e_{abc}. Therefore, the equivalent circuit of the grid-connected SSSG can be as shown in Fig. 2.7, where the LC filter is expected to have impact on the dynamics.

With the system shown in Fig. 2.7, a linearized model is used to evaluate different virtual AVRs from both the steady-state voltage regulation characteristics and the frequency-domain characteristics in [C3]. The results are respectively shown in Fig. 2.8 and Fig. 2.9, where the main parameters are shown in Table 2.2. The following main observations can be summarized:

- For the V-droop control, there is a large deviation between the set-point

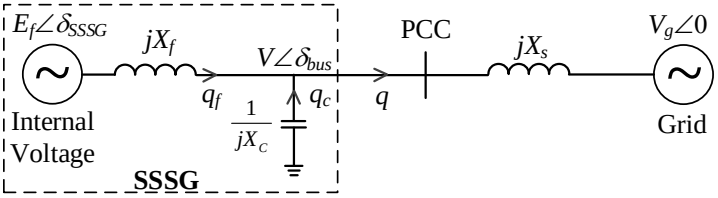

Fig. 2.7: Equivalent circuit of the grid-connected SSSG without virtual winding and inner loop. V_g is the magnitude of grid voltage. X_s is impedacne of line. Source: [C3].

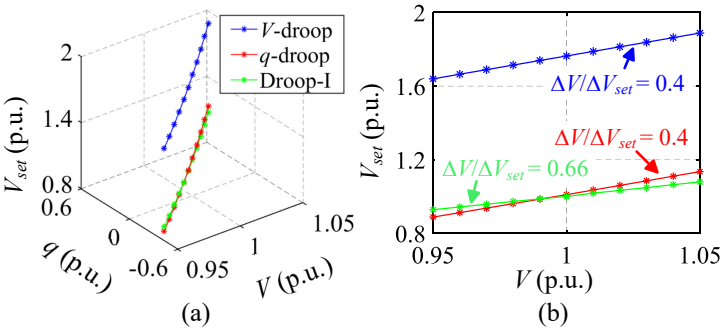

Fig. 2.8: Steady-state voltage regulation characteristics of SSSG without virtual winding and inner loop. Source: [C3].

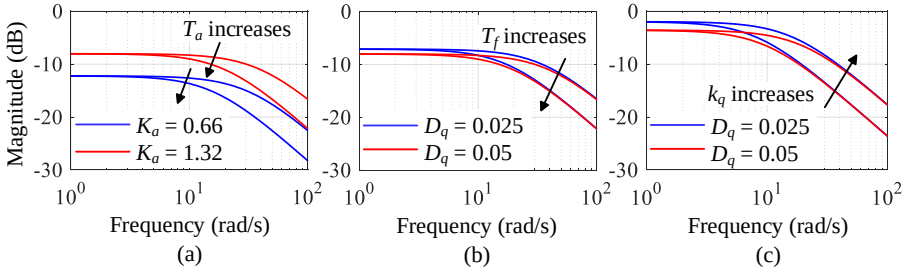

Fig. 2.9: Frequency-domain characteristics of SSSG without virtual winding and inner loop. Source: [C3].

and actual value.

- The droop-I control has the highest sensitivity to the variation of V_{set} (i.e., highest value of $\Delta V/\Delta V_{set}$) and steady-state gain.
- The adjustable parameters have different impact on the bandwith and gain in different virtual AVRs.

The performance of the SSSG with different virtual AVRs are validated by experiments in [C3], where the setup has been shown in 1.9. The step

Table 2.2: Parameters Used to Evaluate the Virtual AVRs

Symbol	Description	Value
f_n	nominal frequency	50 Hz (1 p.u.)
S_n	nominal power	1 kW (1 p.u.)
V_n	nominal line-to-line RMS voltage	80 V (1 p.u.)
L_s	line inductor	2 mH (0.1 p.u.)
L_f	inductor of LC filter	2 mH (0.1 p.u.)
C_f	capacitor of LC filter	10 μF (0.02 p.u.)
K_a	gain in V-droop control	1.32
T_a	time constant in V-droop control	0.083 s
T_f	time constant in q-droop control	0.063 s
k_q	integral gain in droop-I control	26.56
D_q	droop coefficient	0.05 p.u.

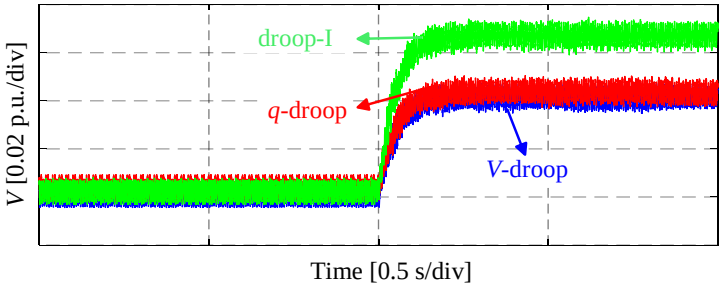

Fig. 2.10: Experimental comparisons of different AVRs responding to a 0.1 p.u. ΔV_{set}. Source: [C3].

response to a 0.1 p.u. ΔV_{set} is presented as an example in Fig. 2.10. As shown, the droop-I control has a larger final value in steady-state than the other methods without sacrificing the responding speed, which is in accordance with the analysis of the steady-state voltage regulation characteristics and the frequency-domain characteristics in Fig. 2.8 and Fig. 2.9.

2.3.2 Impacts of Virtual Impedance and Inner Loops

When considering the virtual impedance and the inner loop, the equivalent circuit of the grid-connected SSSG will change to Fig. 2.11. As shown, the filter is decoupled by an inner loop. Nevertheless, the virtual reactance from the virtual windings X_v (i.e., $X_d = X_q = X_v$) may introduce new influence.

Fig. 2.12 shows the new steady-state voltage regulation characteristics

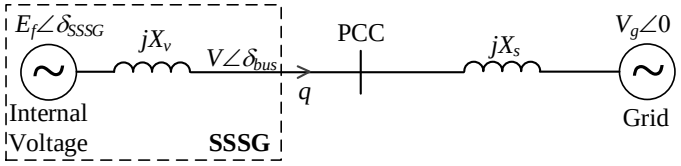

Fig. 2.11: Equivalent circuit of the grid-connected SSSG with virtual winding and inner loop. Source: [C3].

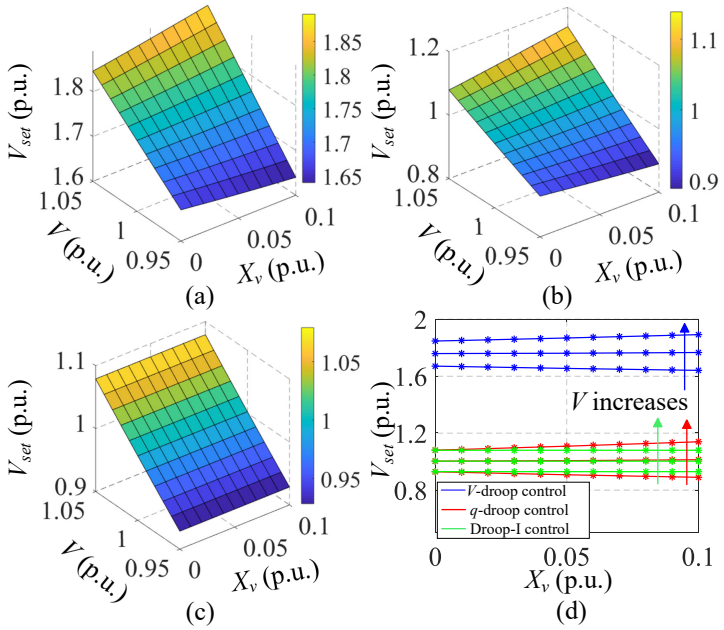

Fig. 2.12: Steady-state voltage regulation characteristics of SSSG with virtual winding and inner loop. Source: [C3].

with the virtual impedance and inner loop. When $X_v = 0$, the q-droop control is identical with the droop-I control. However, as X_v increases, their differences become larger. Especially, a larger V_{set} should be used for the q-droop control in order to keep V at a high level. This is the reason why there is a large voltage decrease in the simulation in Section 2.2. In comparison, the steady-state regulation performance of the droop-I control is not influenced by the virtual impedance.

In summary, the performance of the droop-I control behaves better than the other two strategies both with and without the virtual impedance and inner loop. Therefore, the droop-I control will be used as a default in the following study.

2.4 Electromechanical Oscillation Damping Using 2nd-order Solid-State SG

As mentioned previously, replacing an SG with the 2nd-order model based SSSG may significantly change the dynamics of the power system, where improvements in the electromechanical oscillations damping is observed in some cases. However, in a power system with multiple SGs and therefore multiple electromechanical modes, the impact of the SSSG on each mode is not clear. This topic is investigated in details by participation factors analysis using a small-signal model in [J5]. Which mode can be improved by the SSSG is clarified. Thereafter, with the results of the analysis, an electromechanical oscillation damping strategy is proposed to mitigate the issue.

The IEEE 9-bus test system in Fig. 2.1 and studied cases in Table 2.1 are still used in this section. The local reference frame of G1 is chosen as the common reference frame, where the local variables of G2 and G3 are transformed to the common reference frame in order to build the small-signal model using the following transformations:

$$\boldsymbol{\Delta v} = \boldsymbol{T_t \Delta v_{co}} + \boldsymbol{T_v} \Delta\delta \tag{2.3}$$

$$\boldsymbol{\Delta i_o} = \boldsymbol{T_t \Delta i_{oco}} + \boldsymbol{T_i} \Delta\delta \tag{2.4}$$

where $\boldsymbol{T_t}$, $\boldsymbol{T_v}$, and $\boldsymbol{T_i}$ are the transformation matrices, $\boldsymbol{i_{oco}}$ and $\boldsymbol{v_{co}}$ are the terminal currents and voltages interfaced with the network in the common reference frame, $\boldsymbol{i_o}$ and $\boldsymbol{v}$ are the corresponding variables in the local reference frame, δ is the angle difference between the local and common reference frames. Then, the state-space representation of the generators in the common reference frame can be expressed in the form as [J5]

$$\begin{cases} \boldsymbol{\dot{x}_{pco}} = \boldsymbol{A_{pco} x_{pco}} + \boldsymbol{B_{pco} u_p} + \boldsymbol{B_{pnetco} \Delta i_{oco}} + \boldsymbol{B_s x_{p1}} \\ \boldsymbol{\Delta v_{co}} = \boldsymbol{C_{pco} x_{pco}} + \boldsymbol{D_{pnetco} \Delta i_{oco}} \end{cases} \tag{2.5}$$

where $\boldsymbol{x_{pco}}$ is the state vector of the generator, which includes all the state variables of the (virtual for SSSG) rotor, winding, governor, and AVR, $\boldsymbol{u_p}$ is the vector of the set-point values, $\boldsymbol{x_{p1}}$ is the state vector of G1 representing the connection between the local and the common frames. Thereafter, combing the models of all the generators and the node equation of the network yields the standard state differential equation of the IEEE 9-bus system in the form as

$$\boldsymbol{\dot{x}} = \boldsymbol{Ax} + \boldsymbol{Bu} \tag{2.6}$$

where $\boldsymbol{A}$ is the state transition matrix. According to $\boldsymbol{A}$, there are two electromechanical modes in this three-machine system, which are summarized in Table 2.3.

Table 2.3: Electromechanical Modes of Studied Cases (Source: [J5])

No.	Eigenvalues				Dominant
	Case 1	Case 2	Case 3	Case 4	States
1	-0.05±j8.0	-0.3±j8.1	-2.6±j5.9	-2.4±j5.8	$\Delta\omega$ and $\Delta\delta$ of
2	-0.6±j11.8	-0.5±j12	-0.2±j11.4	-3.1±j6.4	G2 and G3

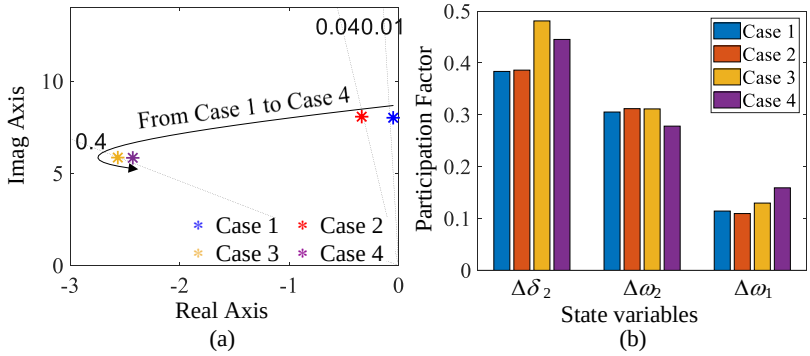

Fig. 2.13: Electromechanical Mode 1 of difference cases given in Table 2.3. (a) Positions in the s-plane. (b) Participation factors of significant states. Subscript "i" (e.g., $i = 1$) means the variables of Gi in Fig. 2.1.Source: [J5].

2.4.1 Participation Factor Analysis

Fig. 2.13 and Fig. 2.14 show the locations of the electromechanical modes in the s-plane and the participation factors of their significant states. It can be seen that although the whole trend of each electromechanical mode from Case 1 to Case 4 are moving to the left by increasing the damping ratio, the details are quite different. For example, the damping ratio is highly increased from Case 2 to Case 3 for Mode 1 while slightly decreased for Mode 2. It means that replacing SG2 with SSSG2 can only damp the oscillation of Mode 1, which on the contrary deteriorates Mode 2. As another example, the damping ratio is highly increased from Case 3 to Case 4 for Mode 2 while it has almost no impact on Mode 1. Moreover, Fig. 2.15 - Fig. 2.17 give the results when Load 1 changes from 5 MW (about 1% of the rated capacity) to 250 MW (about 44% of the rated capacity). Although a larger load makes the elelctromechanical modes in all cases to move to the right, Mode 2 in Case 4 is more sensitive.

These differences between Mode 1 and Mode 2 when replacing an SG with an SSSG have strong relationship with their participation factors and therefore with significant states. In summary, the following can be concluded:

- When significant states of a mode are replaced from SG to SSSG, its

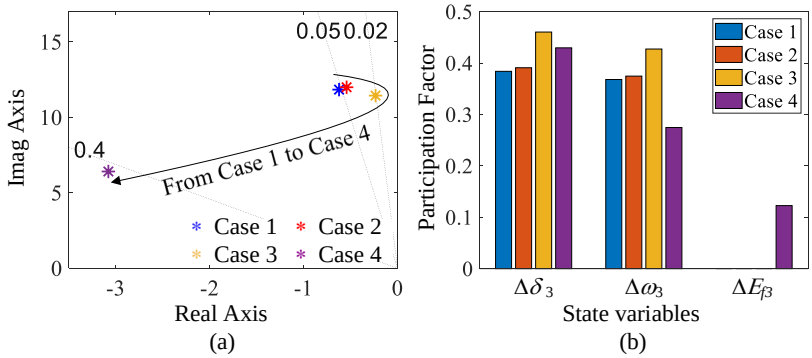

Fig. 2.14: Electromechanical Mode 2 of difference cases. (a) Positions in the s-plane. (b) Participation factors of significant states. E_{f3}: internal voltage of G3. Source: [J5].

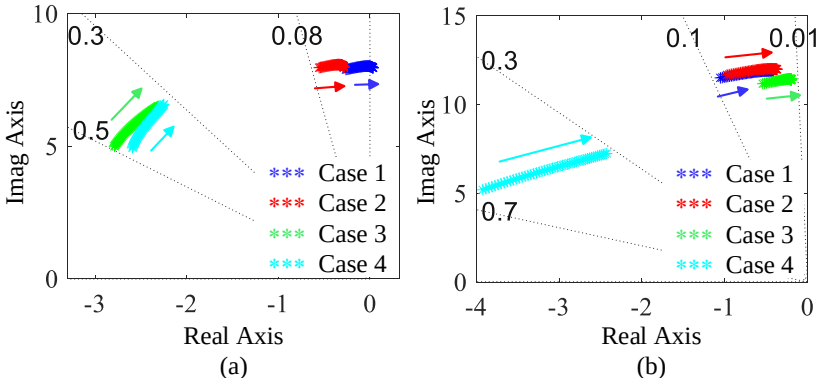

Fig. 2.15: Loci of electromechanical modes when active power of Load 1 increases from 5 MW to 250 MW. (a) Mode 1. (b) Mode 2. Source: [J5].

damping ratio will be improved (e.g., the damping ratio of Mode 1 is increased from Case 1 to Case 2 because $\Delta\omega_1$ is a significant state as shown in Fig. 2.13). If the replaced states are not just significant states but further dominant states, the damping ratio of their corresponding mode will be highly improved (e.g., Mode 1 from Case 2 to Case 3 in Fig. 2.13 and Mode 2 from Case 3 to Case 4 in Fig. 2.14).

- When the replaced states are not significant states and lead the SGs to have larger participation factors in a mode, the damping ratio may be decreased (e.g., the damping ratio of Mode 2 is decreased from Case 2 to Case 3 because states from SSSG2 are not significant states of Mode 2 and the participation factors of $\Delta\delta_3$ and $\Delta\omega_3$ from SG3 are increased as in Fig. 2.14).

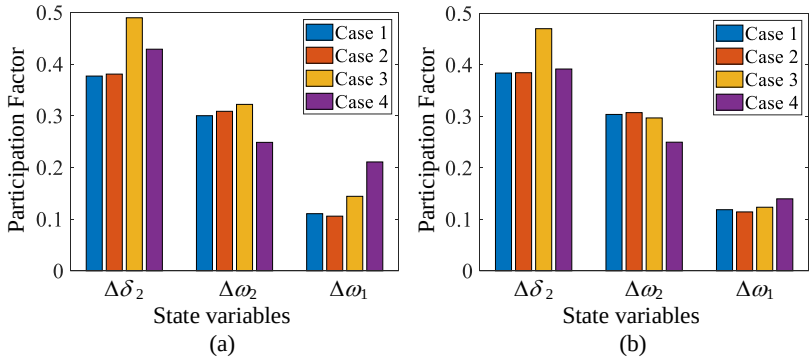

Fig. 2.16: Participation factors of significant states of Mode 1. (a) Active power of Load 1 is 5 MW. (b) Active power of Load 1 is 250 MW. Source: [J5].

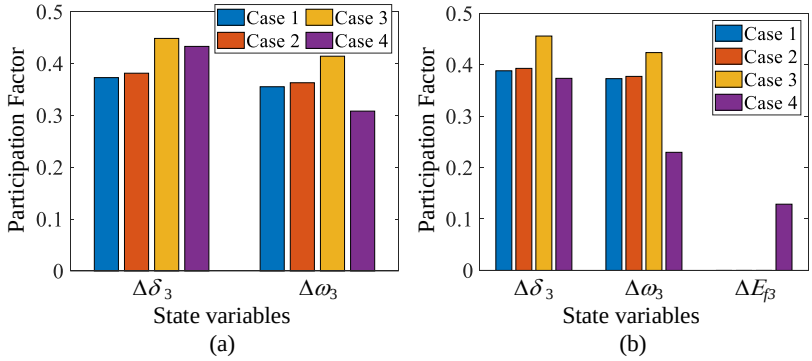

Fig. 2.17: Participation factors of significant states of Mode 2. (a) Active power of Load 1 is 5 MW. (b) Active power of Load 1 is 250 MW. Source: [J5].

- When replacing an SG with an SSSG does not obviously change the participation factors, the electromechanical mode is hardly influenced (e.g., mode 2 from Case 1 to Case 2 in Fig. 2.14).
- The system with SSSGs is more sensitive to parameter variations than the system with SGs due to larger changes in the participation factors.

The analysis on the loci of the electromechanical modes from Case 1 to Case 4 is validated by simulation using Matlab/Simulink of the system shown in Fig. 2.1. As shown before, the dominant states for the two electromechanical modes are $\Delta\delta_2$ and $\Delta\delta_3$, respectively, which then are used to evaluate the dynamics. The waveforms are shown in Fig. 2.18. From Case 2 to Case 3, the oscillation of $\Delta\delta_2$ is highly decreased due to the replacement from SG2 to SSSG2. In comparison, $\Delta\delta_3$ is well damped when SG3 is replaced by SSSG3. These are in accordance with the aforementioned analysis. More

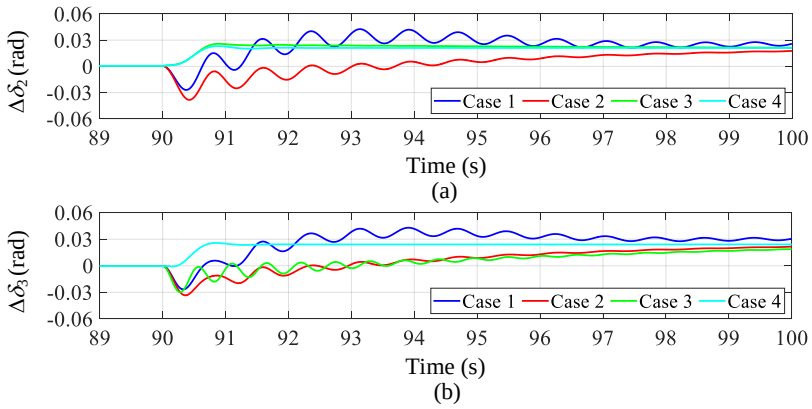

Fig. 2.18: Simulation results of electromechanical modes when there is a 25 MW load disturbance in Load 1 for the system shown in Fig. 2.1. Source: [J5].

studies with respect to the variations of inertia constants can be found in [J5].

2.4.2 Electromechanical Oscillation Damping Strategy

Two basic findings can be concluded from Fig. 2.18. On one hand, it is possible to damp the electromechanical oscillations by replacing the SG with an SSSG. On the other hand, not all the electromechanical oscillations can be damped by an SSSG. It is not practical to use try and error, especially for a large power system with multiple SGs. Therefore, a strategy is proposed to determine which SG should be replaced by the SSSG in order to damp a specific electromechanical mode [J5]. The procedure is summarized as follows:

- Build a small-signal model of the studied power system with SGs.
- Exert the small-signal analysis to identify the electromechanical modes and their dominate states.
- Choose the mode, which is needed to be damped, and then its dominant state.
- Replace the SG, which is corresponding to the dominate state, with an SSSG.
- Check the electromechanical modes of the new system with SSSG in order not to deteriorate the other modes.

To validate the effectiveness of the proposed strategy, Mode 2 is in focus again. Fig. 2.19 compares three different cases, which are Case 1, Case 3, and a new added case. In Case 1, the oscillation is hard to be damped. In Case 3

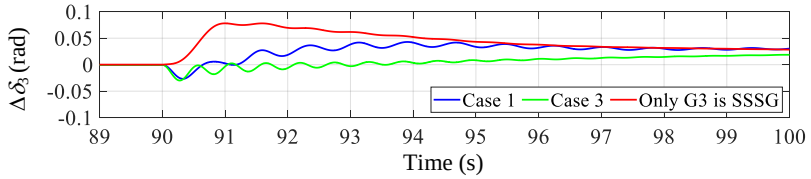

Fig. 2.19: Simulation results of damping $\Delta\delta_3$ using only SSSG3. Source: [J5].

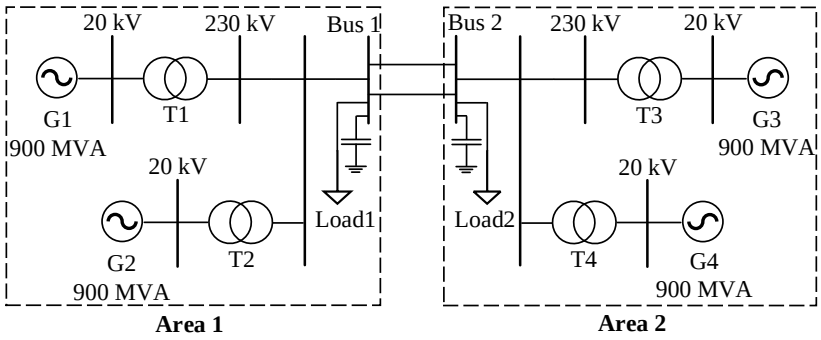

Fig. 2.20: Single-line diagram of the Kundur's four-machine two-area test system. Source: [J5].

when both SG1 and SG2 are replaced by SSSGs, the oscillation is still obvious. In comparison, only replacing SG3 with the SSSG is enough to damp this oscillation. As SG3 provides the dominant state of the studied mode, it will be determined as the one to be replaced by the proposed strategy. Therefore, the proposed strategy will give the right choice.

To demonstrate that the analysis and the proposed method based on the IEEE 9-bus system is still effective in other systems, they are further applied to the Kundur's four-machine two-area test system [74, 75] as shown in Fig. 2.20, which is a typical system to study the electromechanical oscillations. According to the small-signal analysis, this system has one unstable inter-area mode, which is related to all the four generators, and two stable local modes. Two cases are considered, where SG1 and SG4 are replaced by SSSGs, respectively. Fig. 2.21 and Fig. 2.22 show the results in respect to the inter-area and local modes, respectively. As observed, both of SG1 and SG4 can be chosen and replaced by the SSSG in order to damp the inter-area mode as they are related to its significant states. However, replacing SG1 by the SSSG can only influence one of the two local modes. This is because SG1 is not related to the significant states of the other local mode. Similar impact is also observed when SG4 is replaced by the SSSG. This validate that the analysis and the proposed method can be effective also to the Kundur's four-machine two-area test system.

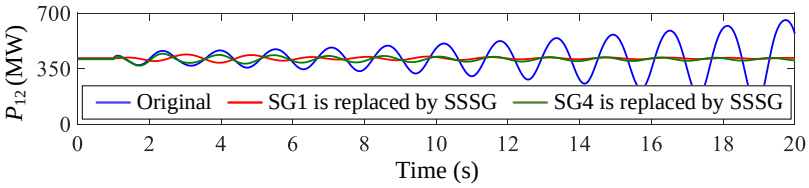

Fig. 2.21: Simulation results of inter-area mode of studied cases. P_{12}: active power from Area 1 to Area 2. Source: [J5].

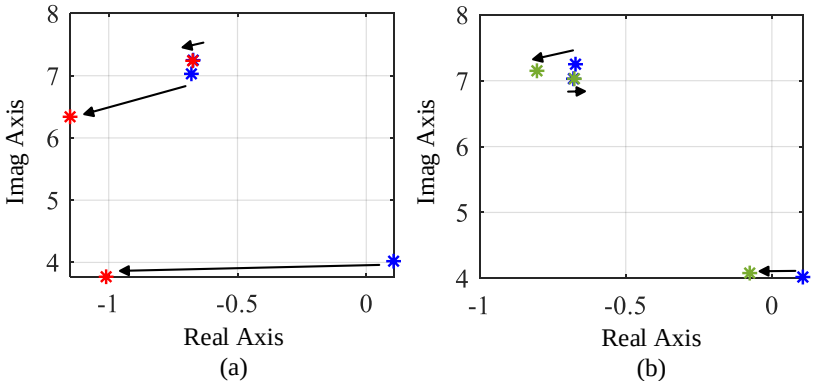

Fig. 2.22: Changes of the electromechanical modes in Kundur's four-machine two-area test system. (a) SG1 is replaced by SSSG. (b) SG4 is replaced by SSSG. Source: [J5].

2.5 Summary

This chapter has focused on the modeling of the SSSG and its impact on the power system. The 6th-order and 2nd-order model based SSSGs are compared with the SGs in different operation conditions. It shows that the 6th-order model based SSSG can well emulate the SG. Nevertheless, the 2nd-order model based SSSG is much simpler and may help to damp the oscillations. Furthermore, three different virtual AVRs are compared in both conditions with and without the virtual reactance and inner loop, which illustrates that the droop-I control can generally provide a better performance. Moreover, the impact of the 2nd-order model based SSSG on damping the electromechanical oscillations has been studied in details by a small-signal analysis. The relationship among the damping, participation factors, and significant states are revealed, based on which a damping strategy is proposed by identifying the significant states of the target mechanical mode. The analysis and the suggested methods have been verified by either simulations or experimental results.

Chapter 3

Characteristics of Solid-State SG Connected to Non-Stiff Grid

3.1 Background

Like in the traditional power system, the indices of RoCoF and frequency deviation are important for the system with the SSSG, and many international and regional standards have already taken them into consideration. For example, IEEE Std 1547-2018 sets the limitations of 0.5 Hz/s over an averaging window of 0.1 s for the RoCoF and $\pm$1.2 Hz for the frequency deviation in continuous operation [76]. These indices have strong relationship with the characteristics of the SSSG (e.g., the RoCoF is mainly determined by the inertia characteristics of the SSSG). Therefore, it is of importance to give a detailed discussion on the characteristics of the SSSG and make clear how the characteristics are dependent on the parameters of the SSSG.

As mentioned before, the Phillips-Heffron model in Fig. 1.5 is a good tool to distinguish the different characteristics by equivalent coefficients in the traditional power system [45,49,50]. However, the SMIB system shown in Fig. 3.1(a) is used and characteristics are evaluated by only set-point variation. In the future power system, the grid structure is expected (as discussed previous) to be more distributed, where the SSSG is typically closer to the local load and can operate without a stiff grid like shown in Fig. 3.1(b) and (c). The change of the grid structure will in return change the characteristics of the SSSG.

Therefore, in this chapter, the equivalent coefficients used in the traditional SMIB system is extended to the analysis using the SSSG [C1,J3]. Specif-

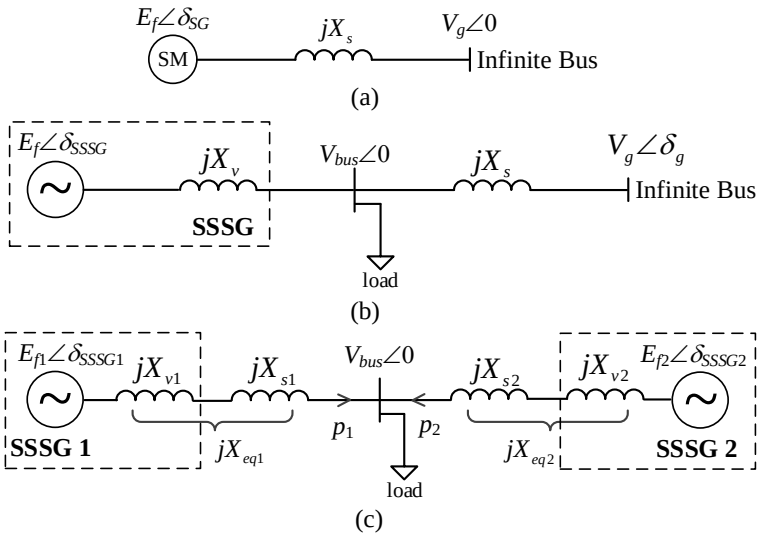

Fig. 3.1: Equivalent circuits of different operation cases. (a) Single-machine-infinite-bus (SMIB) system. (b) Grid-connected SSSG with local load. (c) Paralleled SSSGs system. δ_{SSSG} is the angle difference between SSSG and reference bus, which is load bus in this chapter. Source: [C1,J3].

ically, a equivalent inertia coefficient K_H and a equivalent damping coefficient K_D are used to evaluate the RoCoF and frequency deviation at the beginning of a disturbance (usually before the first peak of the response), and a equivalent synchronizing coefficient K_S can reflect the dynamics over time (usually after the first peak of the response). Both the set-point variation and the load disturbances are investigated in details. Thereafter, the conclusions of the analysis are used to deal with the problem of the dynamic active power sharing in a paralleled SSSGs system. A modified inertia control method is also proposed to improve the performance of the SSSG.

3.2 Equivalent Coefficient Model Analysis

In terms of the three operation cases like shown in Fig. 3.1, the paralleled SSSGs system is a general case, the other two cases can be proved as special ones of the paralleled SSSGs system. Therefore, the system of Fig. 3.1(c) is investigated in details in this section taking SSSG1 as an example.

The small-signal state-space representation of Fig. 3.1(c) can be expressed as [J3]:

$$\begin{cases} \dot{\boldsymbol{x}} = \boldsymbol{A}\boldsymbol{x} + \boldsymbol{B}\boldsymbol{u} \\ \boldsymbol{y} = \boldsymbol{C}\boldsymbol{x} + \boldsymbol{D}\boldsymbol{u} \end{cases} \tag{3.1}$$

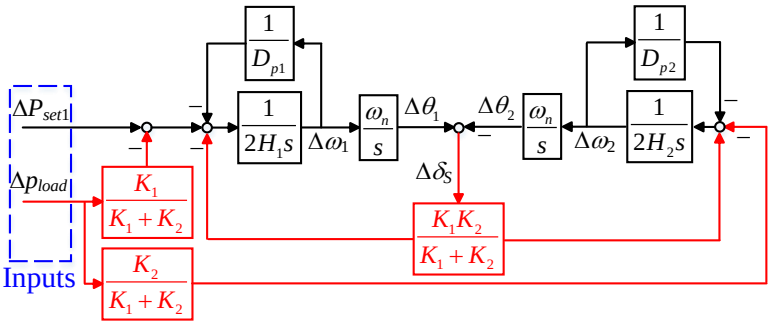

Fig. 3.2: Small-signal model of parallel SSSGs system shown in Fig. 3.1(c). Source: [J3].

where

$$\boldsymbol{x} = \begin{bmatrix} \Delta\omega_1 & \Delta\omega_2 & \Delta\delta_S \end{bmatrix}^T \tag{3.2}$$

$$\boldsymbol{y} = \begin{bmatrix} \Delta p_1 & \Delta p_2 \end{bmatrix}^T \tag{3.3}$$

$$\boldsymbol{u} = \begin{bmatrix} \Delta P_{set1} & \Delta p_{load} \end{bmatrix}^T \tag{3.4}$$

$$\boldsymbol{A} = \begin{bmatrix} -\frac{1}{2H_1 D_{p1}} & 0 & -\frac{K_1 K_2}{2H_1(K_1+K_2)} \\ 0 & -\frac{1}{2H_2 D_{p2}} & \frac{K_1 K_2}{2H_2(K_1+K_2)} \\ \omega_n & -\omega_n & 0 \end{bmatrix} \tag{3.5}$$

$$\boldsymbol{B} = \begin{bmatrix} \frac{1}{2H_1} & 0 & 0 \\ -\frac{K_1}{2H_1(K_1+K_2)} & -\frac{K_2}{2H_2(K_1+K_2)} & 0 \end{bmatrix}^T \tag{3.6}$$

$$\boldsymbol{C} = \begin{bmatrix} 0 & 0 & \frac{K_1 K_2}{K_1+K_2} \\ 0 & 0 & -\frac{K_1 K_2}{K_1+K_2} \end{bmatrix} \tag{3.7}$$

$$\boldsymbol{D} = \begin{bmatrix} 0 & 0 \\ \frac{K_1}{K_1+K_2} & \frac{K_2}{K_1+K_2} \end{bmatrix}^T \tag{3.8}$$

and $\Delta\delta_S = \Delta\delta_{SSSG1} - \Delta\delta_{SSSG2}$, K_1 and K_2 are parameters related to the impedance and steady-state operation point by

$$K_1 = \frac{\partial p_1}{\partial \delta_{SSSG1}} = \frac{E_{f10} V_{bus0}}{X_{eq1}} \cos\delta_{SSSG10} \tag{3.9}$$

$$K_2 = \frac{\partial p_2}{\partial \delta_{SSSG2}} = \frac{E_{f20} V_{bus0}}{X_{eq2}} \cos\delta_{SSSG20} \tag{3.10}$$

A block diagram of the above model is shown in Fig. 3.2, where there are two kinds of input, i.e., the set-point variation ΔP_{set1} and load disturbance Δp_{load}. In the following, both of their impact will be studied, respectively.

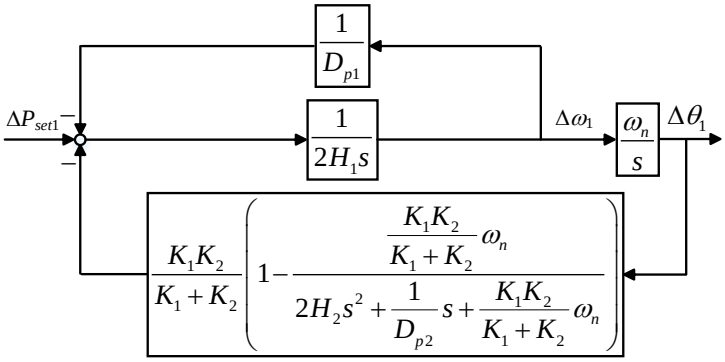

Fig. 3.3: Small-signal model of parallel SSSGs system considering set-point P_{set1} variation. Source: [J3].

3.2.1 Characteristics with Set-Point Variation

When taking ΔP_{set1} as the input, Δp_{load} is set to zero in Fig. 3.2, which can therefore be simplified to the one shown in Fig. 3.3. Therefore, the equivalent coefficients are derived as

$$\begin{cases} K_H = 2H_1 \\ K_D = \dfrac{1}{D_{p1}} \\ K_S = \dfrac{K_1K_2}{K_1+K_2}\left[1-\dfrac{K_1K_2\omega_n/(K_1+K_2)}{2H_2s^2+1/D_{p2}s+K_1K_2\omega_n/(K_1+K_2)}\right] \end{cases} \tag{3.11}$$

According to (3.11), the relationships between the characteristics of the SSSG and various parameters are summarized as

- The equivalent inertia and damping of the SSSG1 are only related to the parameters of itself, i.e., H_1 and D_{p1}, respectively.
- Parameters of SSSG2 do not influence the equivalent inertia and damping characteristics of SSSG1, but will change the synchronizing process via K_S.
- Virtual impedance and line impedance only influence the synchronizing process.

Meanwhile, in (3.11), let $H_2 = +\infty$ and $D_{p2} = 0$, so that SSSG2 becomes an infinite bus. This is the case shown in Fig. 3.1(b) and K_S then becomes

$$K_S = \frac{K_1K_2}{K_1+K_2} \tag{3.12}$$

Further, let $X_{eq2} = 0$, which then becomes the case of the SMIB system shown in Fig. 3.1(a).

Table 3.1: Parameters Used to Investigate the Equivalent Coefficient Model

Symbol	Description	Value
f_n	nominal frequency	50 Hz (1 p.u.)
S_{ni}	nominal power	5 kW (1 p.u.)
V_n	nominal line-to-line RMS voltage	380 V (1 p.u.)
L_{si}	line inductor	1 mH (0.01 p.u.)
L_{fi}	inductor of LC filter	3 mH (0.03 p.u.)
C_{fi}	capacitor of LC filter	10 μF (0.09 p.u.)
H_i	inertia constant	3 s
X_{vi}	virtual synchronous impedance	3 Ω (0.1 p.u.)
D_{pi}	droop coefficient of virtual governor	0.01 p.u.

The islanded paralelled SSSGs experimental setup (shown in Fig. 1.9) is used to investigate the impact of various parameters, where the parameters used in this chapter are listed in Table 3.1. Fig. 3.4 and Fig. 3.5 show the experimental examples corresponding to a step of P_{set1} with 2.5 kW when the inertia constants and droop coefficients are changed. It is observed that a larger H_1 decreases the RoCoF at the beginning of the disturbance, which implies a larger equivalent inertia. In comparison, the variations of H_2 cannot influence the equivalent inertia but do change the dynamics into the steady-state (after the first peak of the response). Similar dynamics can be observed when D_p changes, where the variations of D_{p2} can only influence the performance after about the first peak of the response. These findings validate the conclusions derived by the equivalent coefficients.

3.2.2 Characteristics with Load Disturbance

When taking Δp_{load} as the input, ΔP_{set1} is set to zero. The small-signal model in Fig. 3.2 can be simplified to the one shown in Fig. 3.6. Thereafter, the equivalent coefficients are derived as

$$\begin{cases} K_H = 2H_1 \dfrac{K_1 + K_2}{K_1} \\ K_D = \dfrac{1}{D_{p1}} \dfrac{K_1 + K_2}{K_1} \\ K_S = \dfrac{K_2}{K_1 H_2} [K_2 \dfrac{(H_1/D_{p2} - H_2/D_{p1})s + (K_2 H_1 - K_1 H_2)\omega_n}{2H_2 s^2 + (1/D_{p2})s + K_2 \omega_n} \\ \qquad + K_1 H_2 - K_2 H_1] \end{cases} \tag{3.13}$$

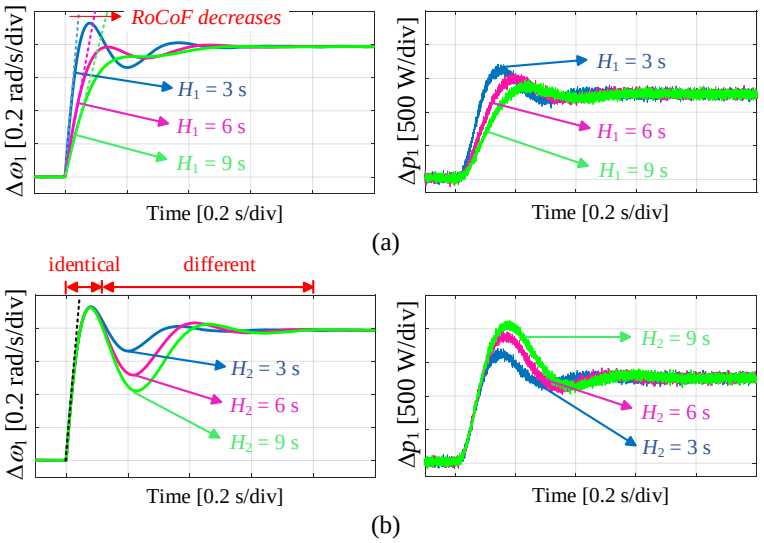

Fig. 3.4: Experimental comparison of responses of SSSG1 responding to a step of P_{set1} with 2.5 kW when the inertia constants are changed. (a) H_1 changes. (b) H_2 changes. Source: [J3].

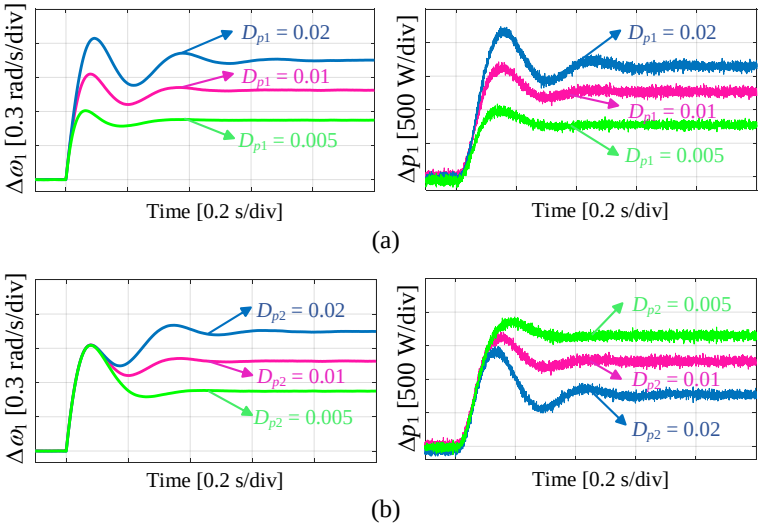

Fig. 3.5: Experimental comparison of responses of SSSG1 responding to a step of P_{0_1} with 2.5 kW when the droop coefficients are changed. (a) D_{p1} changes. (b) D_{p2} changes. Source: [J3].

where the following findings can be summarized:

- The equivalent inertia and damping of the SSSG1 are related to the parameters of itself, i.e., H_1 and D_{p1}, respectively.
- H_2 and D_{p2} of SSSG2 do not influence the equivalent inertia and damp-

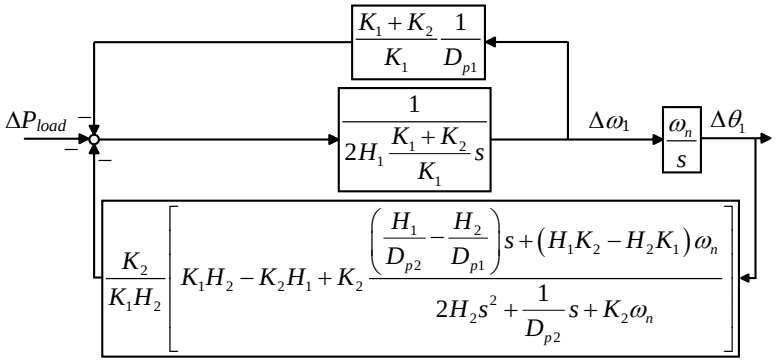

Fig. 3.6: Small-signal model of parallel SSSGs system considering load disturbance. Source: [J3].

ing characteristics of SSSG1, but will change the synchronizing process via K_S.

- Virtual impedance and line impedance will influence all of the three equivalent coefficients.

Similarly, by setting $H_2 = +\infty$ and $D_{p2} = 0$, the special cases of Fig. 3.1(b) can be derived as

$$\begin{cases} K_J = 2H_1\dfrac{K_1+K_2}{K_1} \\ K_D = \dfrac{1}{D_{p1}}\dfrac{K_1+K_2}{K_1} \\ K_S = K_2 \end{cases} \tag{3.14}$$

Fig. 3.7 and Fig. 3.8 show experimental comparisons of dynamics of SSSG1 responding to a load step of 2.5 kW when the inertia constants and droop coefficients are changed, which demonstrates the different impact of H_1 and H_2, D_{p1} and D_{p2} on the inertia and damping characteristics of SSSG1, respectively.

3.2.3 Dynamic Active Power Sharing

Due to the large virtual inertia, the problem of the power oscillation is common in the paralleled SSSGs system. This unbalance of power sharing in the dynamics may harm the stability of the system [77,78]. As an example of application using the equivalent coefficients, the conditions to achieve dynamic active power sharing are studied in [J3].

From the equivalent coefficients model in Fig. 3.6, the dynamics of an SSSG is determined by K_H, K_D, and K_S. Therefore, if all of the three coefficients are identical for the paralleled SSSGs, they are expected to behave with

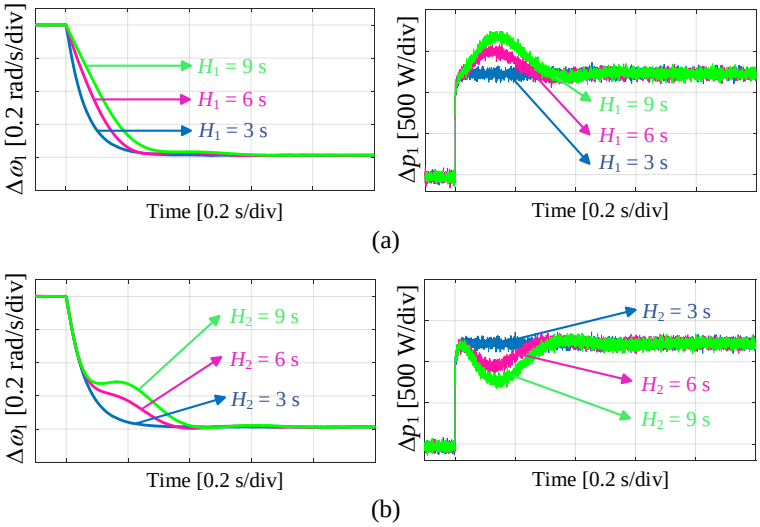

Fig. 3.7: Experimental comparison responding to a load step of 2.5 kW when the inertia constants are changed. (a) H_1 changes. (b) H_2 changes. Source: [J3].

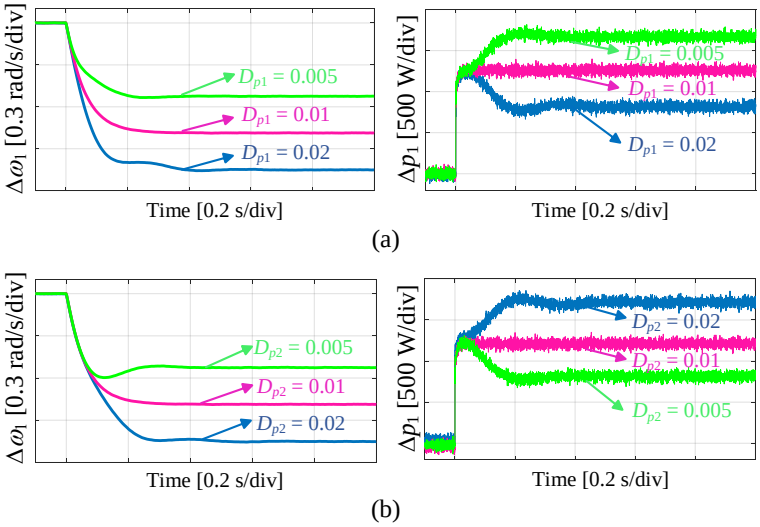

Fig. 3.8: Experimental comparison responding to a load step of 2.5 kW when the droop coefficients are changed. (a) D_{p1} changes. (b) D_{p2} changes. Source: [J3].

the same dynamics as well, which implies that no dynamic unbalance exist in the outputs. According to (3.13), the following conditions can be derived

$$\frac{H_1}{H_2} = \frac{1/D_{p1}}{1/D_{p2}} = \frac{K_1}{K_2} \tag{3.15}$$

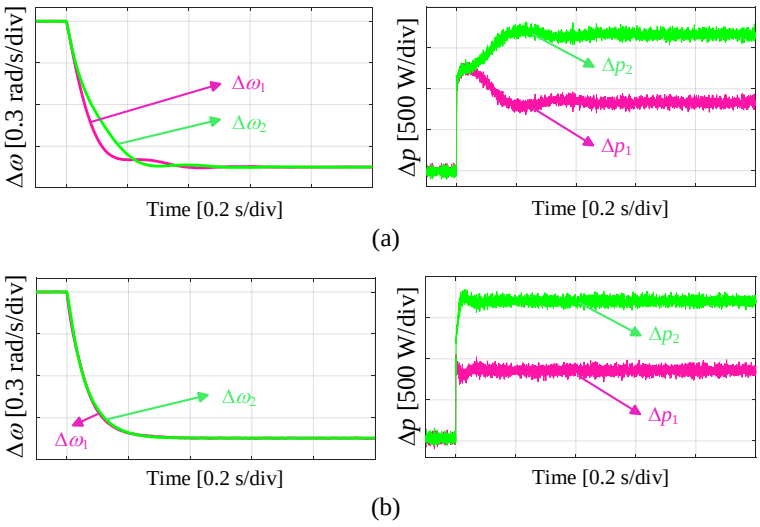

Fig. 3.9: Experimental verification of condition of dynamic active power sharing. (a) Eq. (3.15) is not satisfied. (b) Eq. (3.15) is not satisfied. Source: [J3].

which means that the ratios of the corresponding parameters of the paralleled SSSGs should be equal to each other. It is worth to mention that (3.15) illustrates that the corresponding parameters are not necessary to be exactly identical.

The condition of (3.15) is experimentally verified as in Fig. 3.9. At first, the parameters of SSSG1 and SSSG2 are set as $H_1/H_2 = X_{v1}/X_{v2} = 1$, and $D_{p1}/D_{p2} = 2$, which implies (3.15) is not satisfied and the experimental results are shown in Fig. 3.9(a). The frequencies are not identical and unbalance of active powers can be observed during the transient behavior. Thereafter, H_2 and X_{v2} are changed to satisfy (3.15), where the new experimental results are shown in Fig. 3.9(b). The paralleled SSSGs behave almost with the same dynamics and the oscillation due to the fact that the dynamic active power unbalance is eliminated.

3.3 Modified Inertia Control

According to the aforementioned analysis, it can be noted that the requirements for the parameters of the paralleled SSSGs responding to the set-point variation and load disturbance are different. On one hand, when there is a set-point variation (e.g., ΔP_{0_1}), the equivalent inertia of SSSG1 is only determined by H_1. Thus, a large H_1 may be preferred to limit the RoCoF. On the other hand, when there is a load disturbance, the condition of (3.15) is expected to be guaranteed to decrease the dynamic unbalance of active pow-

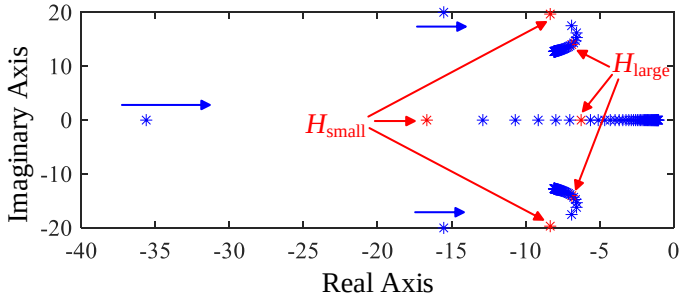

Fig. 3.10: Choices of H_{small} and H_{large} based on the loci analysis. Source: [J3].

ers. Then the parameters of SSSG1 cannot be freely chosen. In order to cope with the conflict of parameters choice between set-point variation and (3.15), a modified inertia control strategy is proposed, which is adaptive according to ΔP_{set}.

With the proposed control, the inertia constant of the SSSG is adaptively changed according to the following equation:

$$H = H_{small} + sgn(|\Delta P_0|)(H_{large} - H_{small}) \tag{3.16}$$

where H equals to H_{small} in normal operation based on (3.15) in order to achieve dynamic active power sharing responding to load disturbance. When a ΔP_0 is detected, H is automatically changed to H_{large} in order to decrease the RoCoF. Thereafter, H is reset to $H = H_{small}$ until the next ΔP_0 comes. Fig. 3.10 presents the choices of H_{small} and H_{large} based on the loci analysis, where H_{large} is set as 5 times of H_{small} for the studied system.

The effectiveness of the proposed modified inertia control is verified by experiments, where the waveforms are shown in Fig. 3.11. The first disturbance is a load disturbance of 2.5 kW, where both the traditional SSSG and the SSSG with the modified inertia control can guarantee good dynamics due to (3.15) being satisfied. Nevertheless, when the second disturbance, i.e., set-point variation, comes in order to restore the frequency to the value before the load disturbance, the traditional SSSG leads to obvious oscillations, which can be well damped by the proposed method.

3.4 Summary

The characteristics of the SSSG connected to a non-stiff power grid is analyzed in this chapter. The equivalent coefficient model used in the traditional power system is extended to the paralleled SSSGs system, and it reveals how various parameters (e.g., inertia constant, droop coefficient, virtual impedance, line impedance) affect the characteristics of the SSSG responding to the variation of set-point and load disturbance.

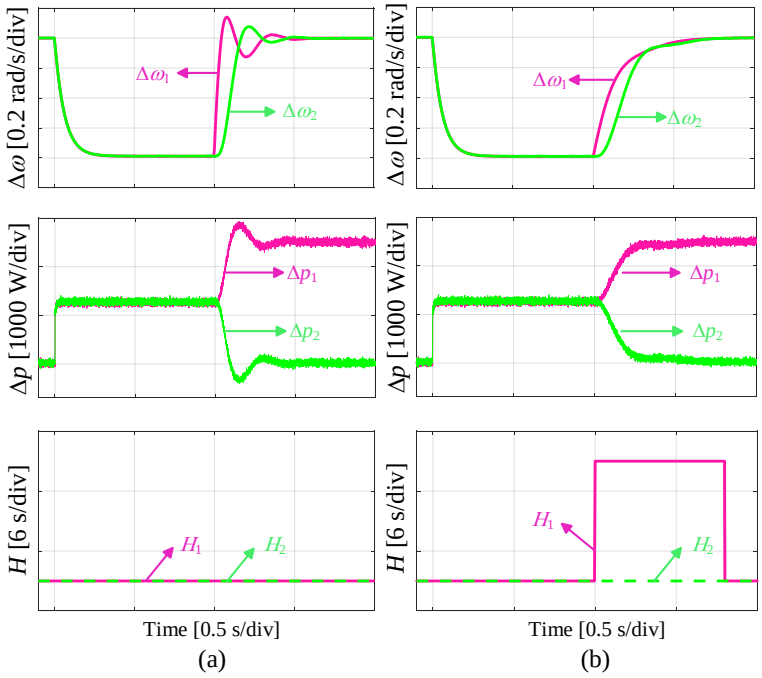

Fig. 3.11: Experimental verification of proposed modified inertia control responding to load step and P_{set1} variation. (a) Traditional SSSG. (b) SSSG with modified inertia control. Source: [J3].

Moreover, this chapter also uses the equivalent coefficients analysis to improve the dynamics of the paralleled SSSGs. It begins with demonstrating that the oscillation due to the unbalance of the dynamic active power can be eliminated, if the ratios of the corresponding parameters between the paralleled SSSGs are identical. Then a modified inertia control is proposed to guarantee a good performance responding to both the variation of set-point and load disturbance, which adaptively change the inertia constant according to the set-point signal. All the analysis and proposed method are verified by experimental results.

Chapter 4

Improved Control Strategies of Solid-State SG

4.1 Background

The analysis in the previous chapters are based on the basic SSSG, where the main motivation is to let the IIG emulate the favorable characteristics of the SG such as the inertia. However, the basic SSSG cannot take full advantages of the control flexibility of the power electronic converter. Just like the inertia characteristics can be achieved by a proper control, other favorable features, which an SG may not have, are also expected to be added into the SSSG to provide superior and robust performance in the grid system.

In Chapter 3, the condition of dynamic active power sharing has been investigated by the equivalent coefficients in order to decrease the oscillations in the paralleled SSSGs system. Nevertheless, the derived conditions are hardly guaranteed exactly in practice due to the requirement of decentralized structure and difficulty to exactly obtain the information of the line impedance. For a general case, it can be shown by root loci analysis that the state variable of the relative rotor angle between the paralleled SSSGs may always introduce a pair of conjugate plural dominated poles, which induce oscillations and then may deteriorate the small-signal stability of the system [52].

Another important issue is the transient angle stability. Like in the traditional SG, the SSSG may also endure instability due to the power angle going across its critical value after a large-signal disturbance, e.g., a short-circuit. However, the behaviors of the SSSG are not the same as the SG due to distinctions in modeling, e.g., the virtual AVR based on the droop-I control. In fact, the dynamics of the droop-I control will decrease the transient stability

margin [26].

This chapter copes with the aforementioned conventional stability issues by proposing improved control strategies on the basis of the SSSG. The corresponding small-signal and large-signal analysis will be presented as well.

4.2 Active Power Oscillation Damping Based on Acceleration Control

In Chapter 3, it has shown that the active power oscillation between paralleled SSSGs can be eliminated if the ratios of the corresponding parameters are identical. Nevertheless, it implies a central manager to simultaneously manage all the paralleled SSSGs, which is inflexible and not practical when a decentralized structure is preferred. Even though there is a central manager, the exact values of the line impedances are hard to get. In order to damp the active power oscillation even when the parameters are mismatched, a damping control based on the acceleration control is proposed in [J2].

4.2.1 Control Principle

In the proposed active power control, the virtual rotor of the basic SSSG (shown in Fig. 1.3(b)) is changed to the block diagram shown in Fig. 4.1, where an additional input signal u is added. The signal u consists of two parts, i.e., a low-frequency component of the acceleration $\dot{\omega}$ to construct the feedback control and a high-frequency component of the output active power p to achieve disturbance suppression. By properly choosing the parameters, the proposed control is equivalent to some special cases given as following:

- Case 1: $k_1 = k_3 = 0$. The proposed control is simplified to the basic SSSG.
- Case 2: $k_1 = 0$. The proposed control is simplified to be the disturbance suppression control.
- Case 3: $k_3 = 0$. The proposed control is simplified to be the acceleration control without disturbance suppression.

Fig. 4.2 compares the frequency characteristics of the islanded paralleled SSSGs system (shown in Fig. 3.1(c)) with the aforementioned methods. It shows that the proposed damping method can well damp the resonant peak of the basic SSSG and provide better performance than the other methods. Fig. 4.3 further shows the sensitivity of the proposed method to the variations of the line impedance, which implies that the proposed method can have good robustness to the variations of the line impedance.

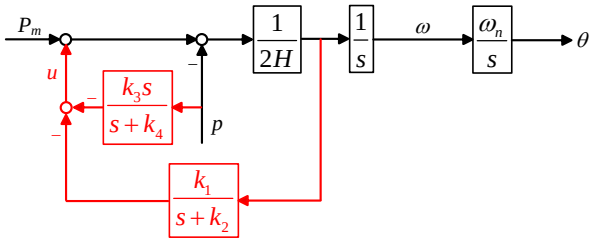

Fig. 4.1: Block diagram of proposed control to damp the active power oscillation. k_1, k_2, k_3, and k_4 are control parameters to be designed. Source: [J2].

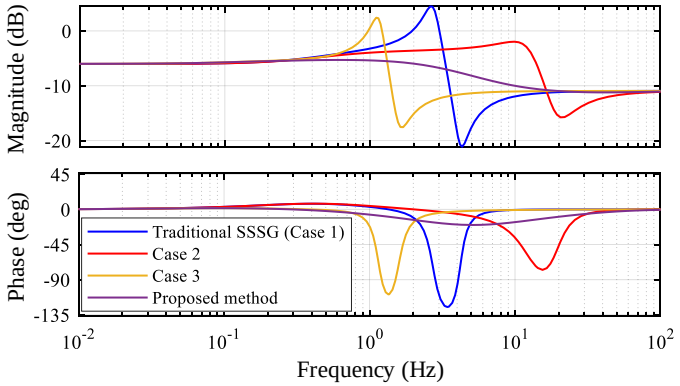

Fig. 4.2: Comparison of frequency characteristics of different control structures. Source: [J2].

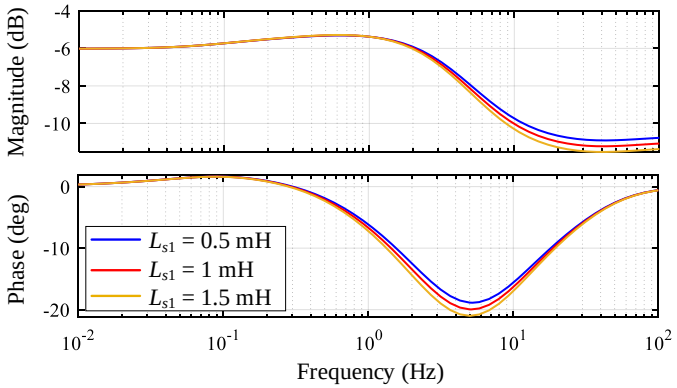

Fig. 4.3: Frequency characteristics of proposed method with different line impedances. Source: [J2].

4.2.2 Small-signal Parameters Design

To design the parameters of the proposed control, a root loci-based small-signal analysis of the islanded paralleled SSSGs system is carried out taking SSSG1 as an example [J2]. For the parameters of acceleration feedback, i.e.,

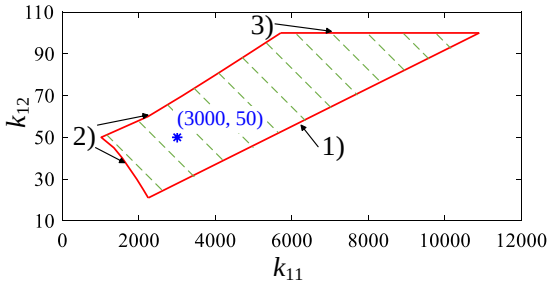

Fig. 4.4: Available region of k_{11} and k_{12} for design of acceleration feedback. Source: [J2].

k_{11} and k_{12} (k_{ij} represents the parameter k_j in Fig. 4.1 for SSSGi), the following requirements should be compromised:

1) Small settling time. E.g., the negative real part of the dominant pole is less than -0.5 in this chapter, which requires small k_{11} and large k_{12}.

2) The existing plural poles are canceled, which requires a large k_{11}.

3) Limitation of high-frequency noise. E.g., the time constant of the acceleration feedback controller is at least 0.01 s in this chapter, which requires a small k_{12}

According to the above requirements, the available parameters region of the acceleration feedback is determined and given in Fig. 4.4, where the marked point is used as design case in this chapter.

Similarly, the following requirements are compromised to determine the parameters of the power feedback, i.e., k_{13} and k_{14}:

1) The existing plural poles are canceled, which requires a large k_{13} and k_{14}.

2) New plural poles should be be introduced, which requires a small k_{13}.

3) Limitation of high-frequency noise. E.g., the time constant of the acceleration feedback controller is at least 0.01 s in this chapter, which requires a small k_{14}

According to the above requirements, the available parameters region of the power feedback is determined and depicted in Fig. 4.5, where the marked point is used as design case in this chapter.

It should be mentioned that, unlike the strict condition given in Chapter 3 to dynamically share the active power, Fig. 4.4 and Fig. 4.5 imply that the parameters can be chosen in a wider range. The proposed method and chosen parameters are experimentally validated using the islanded paralleled SSSGs system (shown in Fig. 1.9), where its main parameters used in this chapter are shown in Table 4.1. In order to make mismatch of the parameters, the

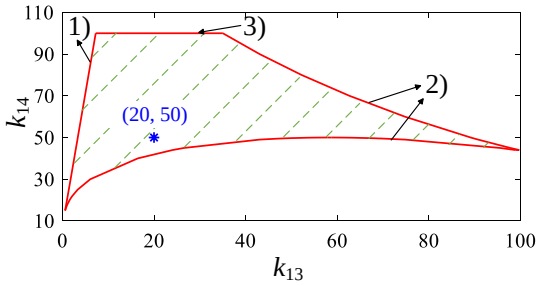

Fig. 4.5: Available region of k_{13} and k_{14} for design of power feedback. Source: [J2].

Table 4.1: Parameters Used to Validate Proposed Damping Method given in Fig. 4.1

Symbol	Description	Value
f_n	nominal frequency	50 Hz (1 p.u.)
S_{ni}	nominal power	5 kW (1 p.u.)
V_n	nominal line-to-line RMS voltage	380 V (1 p.u.)
L_{si}	line inductor	1 mH (0.01 p.u.)
L_{fi}	inductor of LC filter	1.5 mH (0.016 p.u.)
C_{fi}	capacitor of LC filter	20 μF (0.18 p.u.)
H_2	inertia constant of SSSG2	5 s
X_{v2}	virtual synchronous impedance of SSSG2	1 Ω (0.035 p.u.)
D_{p2}	droop coefficient of virtual governor of SSSG2	0.02 p.u.

parameters of SSSG1 are set as $D_{p1} = D_{p2}$, $H_1 = 2H_2$, and $X_{v1} = 3X_{v2}$. In Fig. 4.6, the dynamics of the output active powers with the proposed damping method are compared with some other control strategies. As observed, the oscillation is well damped with the proposed method.

4.3 Enhanced Transient Angle Stability Control

The transient angle stability of the SSSG can be studied using the equal area criterion defined by the power angle curve (p-δ curve). From this point the internal voltage of the SSSG plays an important role because it is directly related to the maximum of the p-δ curve. Actually, it has be shown that the dynamics of the internal voltage has a negative impact on the transient angle stability [26]. Nevertheless, the existing analysis is quite simple and qualitative. To fill up the research gap, a detailed quantitative analysis about how the internal voltage influences the transient angle stability of the SSSG is carried out in [J4].

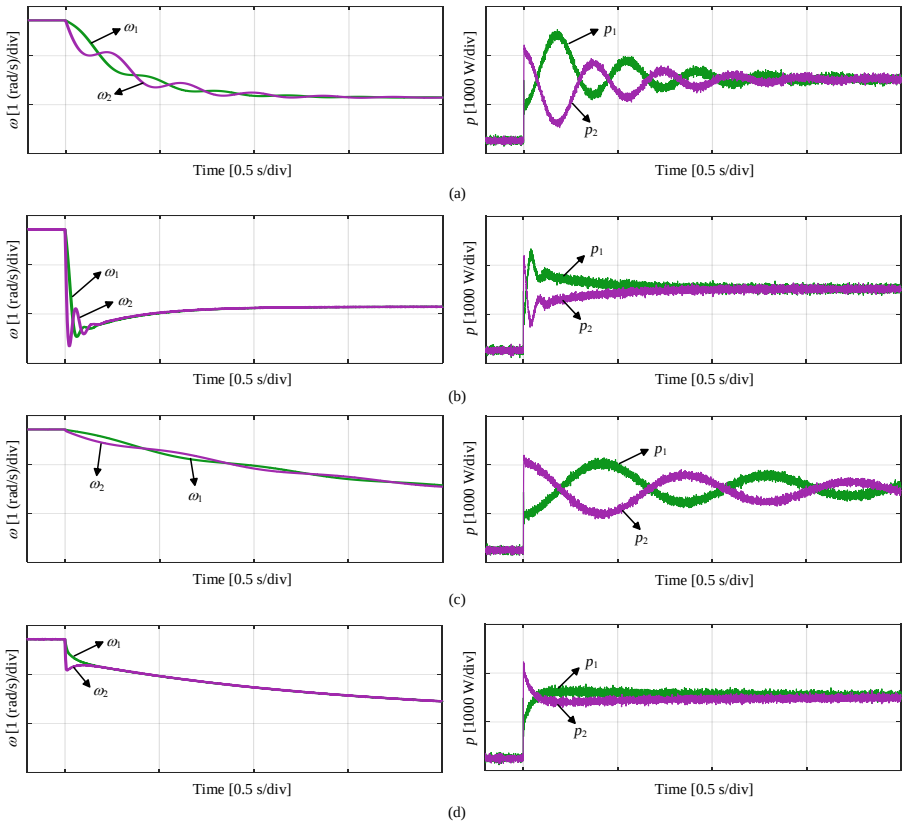

Fig. 4.6: Experimental results of active power with different control strategies. (a) Basic SSSG. (b) Case 2. (c) Case 3. (d) Proposed strategy. Source: [J2].

Moreover, several methods have previously been proposed to enhance the transient angle stability. As listed in Table 4.2, they are compared from different aspects, and all the existing methods seem to have some disadvantages of these aspects. In comparison, a simple and PLL-free method is proposed in [J4], which only use the local information and it will not change the steady-state regulation of pre-defined droop characteristics.

4.3.1 Transient Analysis of Internal Voltage

To analyze the dynamics of the internal voltage, the following simplifications are used:

- Due to the high bandwidth, dynamics of the inner voltage and current loops are neglected [67, 79, 80].
- Due to small time constant, the function of the filter due to the integra-

Table 4.2: Comparison of SSSGs with Improved Large-signal Angle Stability (Source: [J4])

Methods	Simplicity	Steady-state regulation	PLL-free	Local information
[67,68]	x	√	√	√
[64]	x	√	√	x
[26]	√	x	√	√
[63,65,66]	√	√	x	√
Proposed method [J4]	√	√	√	√

tor in the droop-I based virtual AVR is neglected [20,26,36,65].

Thereafter, the relationship between the output active power p, the internal voltage E_f, and the power angle δ_{SSSG} of the grid-connected SSSG system (shown in Fig. 2.11) can be derived as

$$E_f = \frac{\sqrt{(D_q V_g \cos\delta_{SSSG} - X_s)^2 + 4D_q X_s (V_{set} + D_q Q_{set})}}{2D_q} + \frac{D_q V_g \cos\delta_{SSSG} - X_s}{2D_q} \tag{4.1}$$

$$p = \frac{V_g sin\delta_{SSSG} \sqrt{(D_q V_g \cos\delta_{SSSG} - X_s)^2 + 4D_q X_s (V_{set} + D_q Q_{set})}}{2D_q X_s} + \frac{D_q V_g^2 \sin\delta_{SSSG} \cos\delta_{SSSG} - X_s V_g \sin\delta_{SSSG}}{2D_q X_s} \tag{4.2}$$

Thereafter, the following findings can be proved [J4]:

- E_f is a monotonically decreasing function of δ_{SSSG}, a monotonically increasing function of the grid voltage V_g with $\delta_{SSSG} \in [0, \pi/2]$ and a monotonically decreasing function of V_g with $\delta \in [\pi/2, \pi]$.
- The dynamics of E_f enlarge the acceleration area and lessen the deceleration area. Nevertheless, the latter is more obvious than the former. Their differences become less as the depth of the voltage sag increases.

Fig. 4.7 shows the phase portrait of the basic SSSG (shown in Fig. 1.3(b)) with different depths of voltage sag, where the used parameters are listed in Table 4.3. As observed, due to the decreasing of E_f, the transient stability margin of the SSSG is decreased as well. When V_g decreases to 0.6 p.u., the system is already unstable, while it is still stable if the dynamic of E_f is not

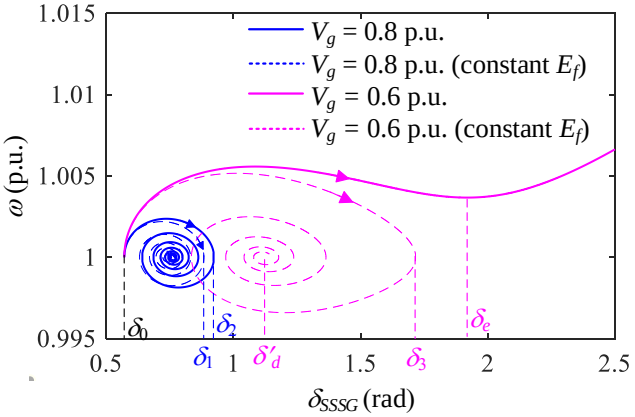

Fig. 4.7: Phase portrait in δ_{SSSG}-ω plane with different voltage sag. Source: [J4].

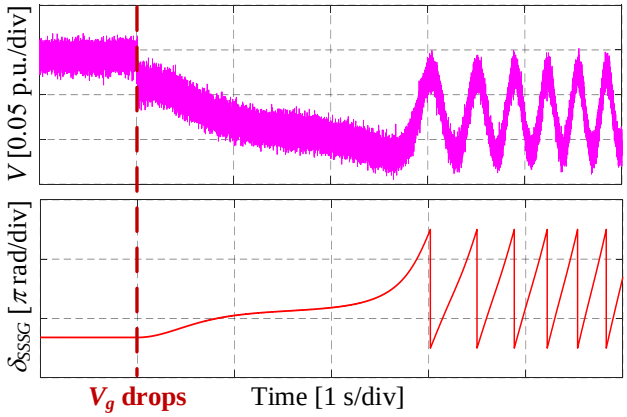

Fig. 4.8: Experimental results of basic SSSG when V_g drops to 0.6 p.u. V is the magnitude of capacitor voltage, and is used to represent E_f due to the fact that V is controlled as E_f by the inner voltage and current loops. Source: [J4].

considered. The grid-connected SSSG experimental setup shown in Fig. 1.9 is used to demonstrate the impact of E_f. As shown in Fig. 4.8, E_f decreases as δ_{SSSG} increases. As mentioned before, this dynamics of E_f decreases the transient stability margin to make the system unstable in the case where V_g drops to 0.6 p.u. In comparison, Fig. 4.9 shows the experimental results when the virtual AVR is not active, and it represents a stable system.

4.3.2 Transient Angle Stability Control and Large-Signal Analysis

To enhance the transient angle stability of the SSSG, a simple method is proposed, where the control block diagram of the basic SSSS (shown in Fig.

Table 4.3: Parameters Used in Studying Transient Angle Stability of SSSG

Symbol	Description	Value
ω_n	nominal frequency	100π rad/s (1 p.u.)
S_n	nominal power	1 kW (1 p.u.)
V_n	nominal line-to-line RMS voltage	80 V (1 p.u.)
ω_g	grid frequency	1 p.u.
V_g	grid voltage	1 p.u.
L_f	inductor of LC filter	2 mH (0.1 p.u.)
C_f	capacitor of LC filter	10 μF (0.02 p.u.)
L_g	line inductor	11 mH (0.52 p.u.)
P_{set}	set-point value of active power	1 p.u.
ω_{set}	set-point value of frequency	1 p.u.
V_{set}	set-point value of voltage	1.01 p.u.
Q_{set}	set-point values of reactive power	0 p.u.
D_p	droop coefficient of virtual governor	0.09 p.u.
H	inertia constant	9 s
D_q	droop coefficient of virtual AVR	0.05 p.u.
X_v	virtual synchronous reactance	0 p.u.
k_q	integral gain of virtual AVR	110

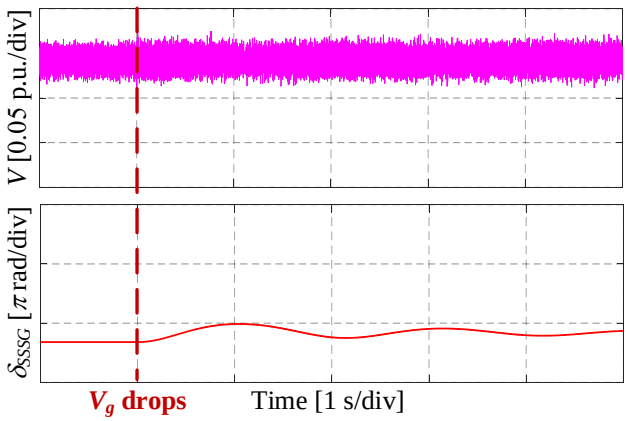

Fig. 4.9: Experimental results of basic SSSG when V_g drops to 0.6 p.u. and virtual AVR is disabled. Source: [J4].

1.3(b)) is changed to one shown in Fig. 4.10. Compared with the traditional virtual AVR based on the droop-I control, in the proposed method, a new signal which is related to the power difference is introduced to virtual

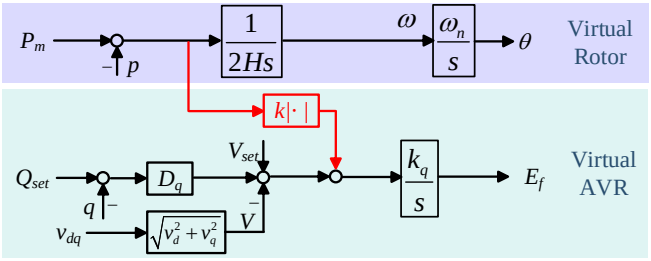

Fig. 4.10: Block diagram of proposed enhanced transient angle stability control of SSSG. Source: [J4].

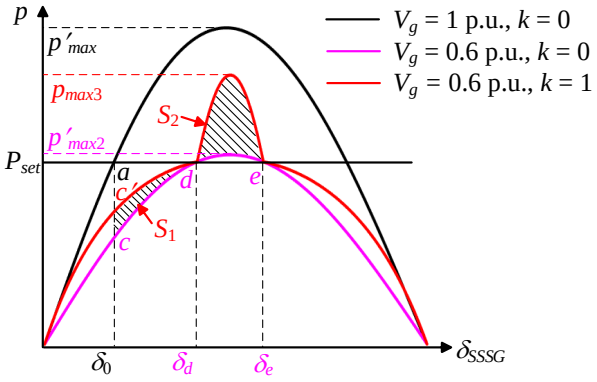

Fig. 4.11: Impact of proposed method on p-δ_{SSSG} curve take $k = 1$ as an example. Source: [J4].

AVR by the operator of absolute value. It can be proved that, with the proposed method, the output power p is monotonically increasing as the gain k increases except the equilibria $p = P_{set}$ [J4]. Then, the functions of the proposed method can be explained by the p-δ_{SSSG} curve as shown in Fig. 4.11. Compared with the traditional virtual AVR (i.e., $k = 0$), the proposed method make the initial operation point after the disturbance occur to go up from point c to c'. As a result, the acceleration area is decreased by S_1. Meanwhile, after δ_{SSSG} go across the equilibrium point d, the maximum value of the p-δ curve is increased from p'_{max2} to p'_{max3}, which leads the deceleration area is increased by S_2. All together, the transient angle stability of the SSSG is improved.

Fig. 4.12 shows the phase portrait with the proposed method with different gain k. Compared with the traditional virtual AVR (i.e., $k = 0$), the deviation of ω from the equilibrium is decreased when $k = 0.3$ although the system is still unstable. As k increases to 0.6 and 0.9, the systems are stable, and the deviations of ω and δ_{SSSG} become smaller and smaller, which implies a better transient stability. A proper range of k is $k \in [0.54, 0.94]$ for the grid-connected SSSG system specified in Fig. 2.11 based on an iterative

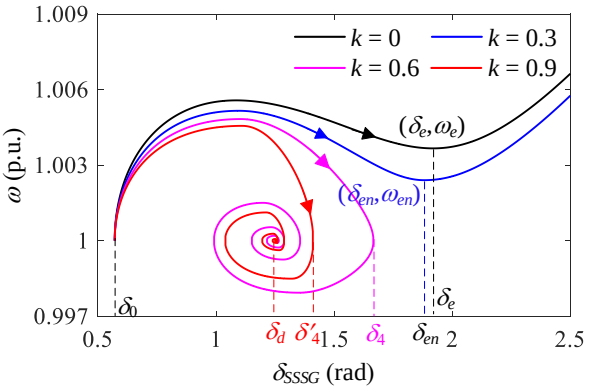

Fig. 4.12: Phase portrait with the proposed method with different gains k in Fig. 4.10. Source: [J4].

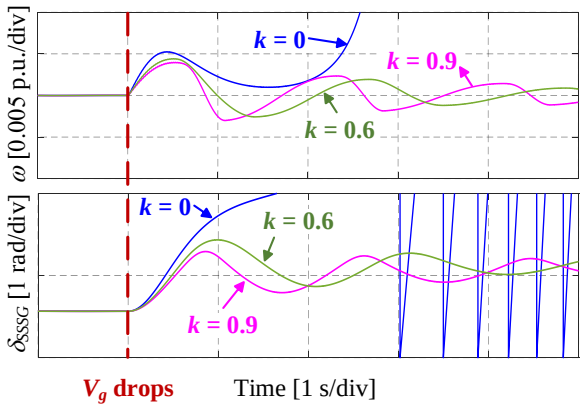

Fig. 4.13: Experimental results with the proposed method with different gains k when V_g decreases to 0.6 p.u. Source: [J4].

algorithm [J4].

The effectiveness of the proposed method is verified by experimental results as shown in Fig. 4.13. As observed, the original system is unstable, while the cases when $k = 0.6$ and $k = 0.9$ are stable. Furthermore, it is also observed that the damping of the oscillation is hardly changed, which proves that the proposed method exerts its function by changing the acceleration and deceleration areas rather than changing the damping.

4.4 Summary

This chapter copes with the advanced control of SSSG in order to provide more favorable features beyond the SG, where two main issues are considered. Firstly, a damping strategy is proposed based on the acceleration con-

trol with a power disturbance suppression. Thereafter, the power oscillations between parallel SSSGs are well damped even if their parameters are mismatched. The small-signal stability analysis is used to help designing the parameters. Secondly, the transient angle stability is studied. A detailed quantitative analysis of the internal voltage is carried out in order to reveal how its transient dynamics will deteriorate the transient angle stability of the SSSG. A simple method is proposed to enhance the transient angle stability, where the principle is to simultaneously decrease the acceleration area and increase the deceleration area. All the analysis and proposed methods have been verified by experimental results.

Chapter 5

Multivariable Feedback Control of Solid-State SG

5.1 Background

Looking back to the motivation of the basic SSSG, it is proposed to control the IIGs to emulate the SGs. Then the improved methods are developed from the basic SSSG. However, paying too much attentions on the basic SSSG may limit the ideas and possibilities on how to develop and improve the SSSG operation. There are usually two important assumptions in the basic SSSG. One is that the DC source is ideal, and the other is that different loops are decoupled and thereby can be designed separately. Therefore, most of the improved SSSGs also hold these two assumptions. These assumptions bring benefits in analysis and design by using classic control theory for single-input single-output (SISO) system such as root loci and frequency-domain methods. However, the performance of the SSSG is limited as the important coupling information is missing.

It is noted that the SSSG is a special form of the grid-forming converter, which provides the possibility of design an SSSG from the perspective of grid-forming converter. Therefore, this chapter begins with studying a general grid-forming converter, and then embodies it to the SSSG. The topology of a grid-forming converter and its open-loop equivalent circuit in *d-q* frame is shown in Fig. 5.1. Unlike the usual assumption of an ideal DC source, a controlled current source i_u is used in this chapter in order to take the dynamics of the DC capacitor C_{dc} into consideration [81]. The dynamics of the DC voltage is dominated by

$$\dot{v}_{dc} = \frac{\omega_n}{C_{dc}} i_u - \frac{\omega_n E i_d}{C_{dc} v_{dc}} \tag{5.1}$$

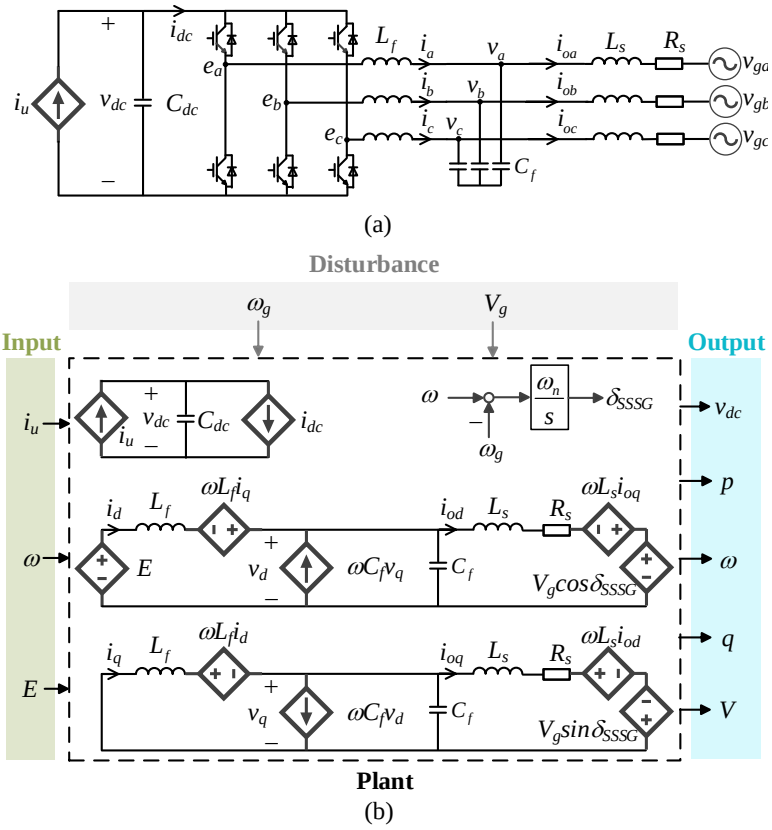

Fig. 5.1: Grid-forming converter (a) Topology. (b) MIMO open-loop equivalent circuit in *d*-*q* frame. The variables are in accordance with the ones defined in Fig. 1.3(b). Source: [J6].

where v_{dc} is the DC voltage. It shows that the AC dynamics are contained in the DC dynamics by Ei_d. Therefore, it is possible to improve the performance of the grid-forming converter by coupling the DC and AC sides. In addition to the DC current i_u, the basic function for a grid-forming control is to provide the frequency and voltage signals, i.e., ω and E. Meanwhile, the DC voltage v_{dc}, active power p and frequency ω_u, reactive power q and terminal voltage V are signals, which are usually paid attention to. Therefore, the grid-forming converter is actually a MIMO system with three inputs and five outputs, where design methods based on the classic control such as root locus and loop shaping may not provide the most optimal and robust performance.

In [J6], a generalized configuration of the grid-forming converter is proposed based on the multivariable feedback control, based on which a new MIMO-SSSG control is specified. The proposed MIMO-SSSG control can not only maintain the inertia and droop characteristics, but can also provide su-

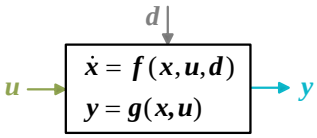

Fig. 5.2: MIMO open-loop state-space model of grid-forming converter. Source: [J6].

perior and robust performance taking advantages of the DC/AC couplings. To this end, how the control parameter design of the proposed MIMO-based SSSG can be transformed into a standard H_∞ synthesis is also discussed [J6], where multiple parameters can be tuned simultaneously in an optimized way.

5.2 Generalized Control Structure

The equivalent circuit of the grid-forming converter in Fig. 5.1 can be converted into the state-space model shown in Fig. 5.2, where $\boldsymbol{x}$, $\boldsymbol{u}$, $\boldsymbol{y}$, and $\boldsymbol{d}$ are the vectors of states, inputs, outputs, and disturbances in accordance with Fig. 5.1, which are defined as

$$\boldsymbol{x} = \begin{bmatrix} i_d & i_q & v_d & v_q & i_{od} & i_{oq} & \delta_{SSSG} & v_{dc} \end{bmatrix}^T \tag{5.2}$$

$$\boldsymbol{u} = \begin{bmatrix} i_u & \omega & E \end{bmatrix}^T \tag{5.3}$$

$$\boldsymbol{y} = \begin{bmatrix} v_{dc} & p & \omega & q & V \end{bmatrix}^T \tag{5.4}$$

$$\boldsymbol{d} = \begin{bmatrix} \omega_g & V_g \end{bmatrix}^T \tag{5.5}$$

where the output signals p, q, V are expressed by the state variables as

$$p = v_d i_{od} + v_q i_{oq} \tag{5.6}$$

$$q = -v_d i_{oq} + v_q i_{od} \tag{5.7}$$

$$V = \sqrt{v_d^2 + v_q^2} \tag{5.8}$$

By applying a multivariable feedback control, the proposed generalized configuration of the grid-forming converter is shown in Fig. 5.3, where $\boldsymbol{\Phi} = (\phi_{ij})_{3\times5}$ is called control transfer matrix. It is noticed that, unlike the tradition to decouple different loops as SISO systems, $\boldsymbol{\Phi}$ is a 3×5 matrix, which works on the vector of error signals and generates the vector of inputs as a MIMO matrix. Actually, the basic SSSG shown in Fig. 1.3(b) can be seen as a special case of the proposed configuration by simplifying the MIMO system to decoupled systems as shown in Fig. 5.4 with the control transfer matrix

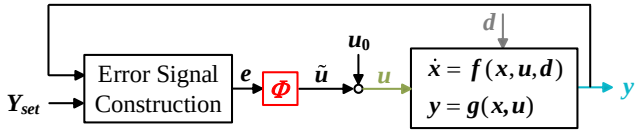

Fig. 5.3: Block diagram of proposed generalized configuration of grid-forming converter. Source: [J6].

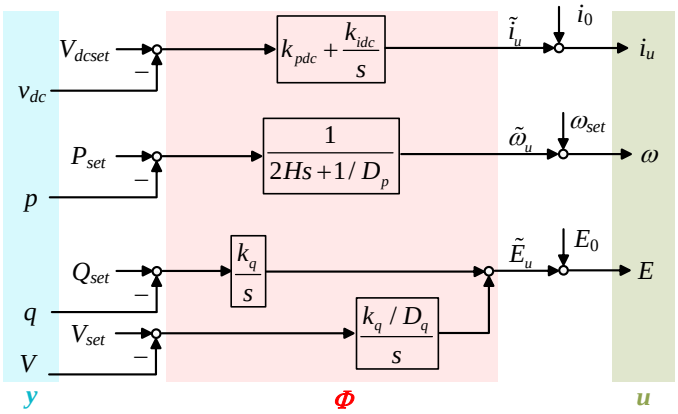

Fig. 5.4: Block diagram of basic SSSG of Fig. 1.3(b) in the form of proposed generalized configuration. Source: [J6].

being

$$\mathbf{\Phi} = \begin{bmatrix} k_{pdc} + k_{idc}/s & 0 & 0 & 0 & 0 \\ 0 & \frac{1}{2Hs+1/D_p} & 0 & 0 & 0 \\ 0 & 0 & 0 & k_q/s & \frac{k_q/D_q}{s} \end{bmatrix} \tag{5.9}$$

where the DC voltage control is assumed to be a PI controller.

The proposed generalized configuration has several advantages as following:

- Various existing grid-forming controls such as droop control, SSSG control, power synchronization control, etc., and their improved form are unified in the control transfer matrix $\mathbf{\Phi}$ working on different linear or nonlinear error signals. As an example, Table 5.1 summarizes the employed control transfer matrices for different SSSGs.
- Comparisons between various grid-forming controllers are straightforward.
- Performance of different loops including both AC and DC sides can be optimized simultaneously.
- New grid-forming controls can be motivated.

Table 5.1: Summary of Control Transfer Matrices Corresponding to Different SSSGs

Feedback Signals $\boldsymbol{y}$	v_{dc}	p	ω	q	V	v_{dc}	p	ω	q	V	v_{dc}	p	ω	q	V
Transfer Matrix ϕ_{ij}	ϕ_{11}	ϕ_{12}	ϕ_{13}	ϕ_{14}	ϕ_{15}	ϕ_{21}	ϕ_{22}	ϕ_{23}	ϕ_{24}	ϕ_{25}	ϕ_{31}	ϕ_{32}	ϕ_{33}	ϕ_{34}	ϕ_{35}
SSSG-1 [C1], [C3]	PI	0	0	0	0	0	IF	0	0	0	0	0	0	0	IF
SSSG-2 [58,82], [C3]	PI	0	0	0	0	0	IF	0	0	0	0	0	0	PI	PI
SSSG-3 [66]	PI	0	0	0	0	0	IF	0	0	0	0	0	P	P	0
SSSG-4 [65]	PI	0	0	0	0	0	IF	IF	0	0	0	0	0	P	0
SSSG-5 [27,63,82]	PI	0	0	0	0	0	IF	IF	0	0	0	0	0	PI	PI
SSSG-6 [26]	PI	0	0	0	0	0	IF	0	0	IF	0	0	0	I	I
SSSG-7 [52]	PI	0	0	0	0	0	O×PD	0	0	0	0	0	0	I	I
SSSG-8 [27]	PI	0	0	0	0	0	IF×PD	0	0	0	0	0	0	PI	PI
SSSG-9 [83]	PI	0	0	0	0	IF×PD	IF×PD	0	0	0	0	0	0	P	0
SSSG-10 [82]	PI	0	0	0	0	0	IF_1 {$\text{IF}_1\times\text{IF}_2\times$D}	0	0	0	0	0	0	PI	PI
SSSG-11 [J2]	PI	0	0	0	0	0	O×PD {O×IF×PD×D}	0	0	0	0	0	0	I	I
SSSG-12 [82,84]	PI	0	0	0	0	0	$\text{O}\times\text{PD}_1$ {$\text{O}\times\text{IF}\times\text{PD}_2\times$D}	0	0	0	0	0	0	PI	PI
Generated Inputs $\boldsymbol{u}$	i_u					ω					E				

P: Proportional controller k, I: Integral controller $\frac{1}{Ts}$, D: Derivative controller Ts, PI: Proportional integral controller $k(1+\frac{1}{Ts})$, PD: Proportional derivative controller $k(1+Ts)$, IF: Inertia factor $\frac{k}{Ts+1}$, O: Oscillatory factor $\frac{k}{T^2s^2+2T\xi s+1}$.
{}: the term is only applied to the feedback channel.

Detailed discussions about the above advantages of the proposed generalized configuration and the control transfer matrix can be found in [J6].

5.3 H_∞ Based Parameters Optimization

As mentioned before, the existing grid-forming controls are almost based on SISO loops, which can also be seen from Table 5.1 that the control transfer matrices are quite sparse. This has inspired to improve the performance of the SSSG by proper designing the coupling terms. Therefore, a MIMO-SSSG is proposed based on the generalized configuration of the grid-forming converter, where the following principles are considered to construct the control

transfer matrix:

- ϕ_{11} is chosen as a PI controller to achieve zero-error in DC voltage as

$$\phi_{11} = k_{pdc} + \frac{k_{idc}}{s} \tag{5.10}$$

- ϕ_{22} is chosen as an LPF multiplying the p-f droop coefficient D_p in order to keep the inertia and steady-state droop characteristics as

$$\phi_{22} = \frac{D_p k_{22}}{s + k_{22}} \tag{5.11}$$

- The third column is set as zero to avoid using PLL as

$$\phi_{13} = \phi_{13} = \phi_{33} = 0 \tag{5.12}$$

- ϕ_{34} and ϕ_{35} are chosen as I controllers to keep the q-V droop characteristics as

$$\phi_{34} = D_q \phi_{35} = \frac{k_{34}}{s} \tag{5.13}$$

- The ratio between ϕ_{24} and ϕ_{25} is set to q-V droop coefficient D_q in order not to influence the steady-state p-f droop characteristics as

$$\phi_{24} = D_q \phi_{25} = k_{24} \tag{5.14}$$

- Other coupling terms are chosen as simple P controllers

Based on the above descriptions, the proposed control transfer matrix is expressed as

$$\mathbf{\Phi} = \begin{bmatrix} k_{pdc} + k_{idc}/s & k_{12} & 0 & k_{14} & k_{15} \\ k_{21} & D_p k_{22}/(s + k_{22}) & 0 & k_{24} & k_{24}/D_q \\ k_{31} & k_{32} & 0 & k_{34}/s & \frac{k_{34}/D_q}{s} \end{bmatrix} \tag{5.15}$$

which has the following features:

- Favorable characteristics of the basic SSSG, i.e., inertia and droop regulation, are kept.
- The order of the system is not increased compared with the basic SSSG unlike other improved forms. Nevertheless, the performance is expected to be improved by the coupling terms.

The proposed control transfer matrix has several control parameters to be designed. The traditional design methods used in the SSSG are based on the classic control theory such as root locus and loop shaping, which are not suitable for an MIMO system in terms of performance. In the following, it shows how this problem can be transformed into a standard fixed structure H_∞ optimization problem, where all the control parameters can be tuned simultaneously.

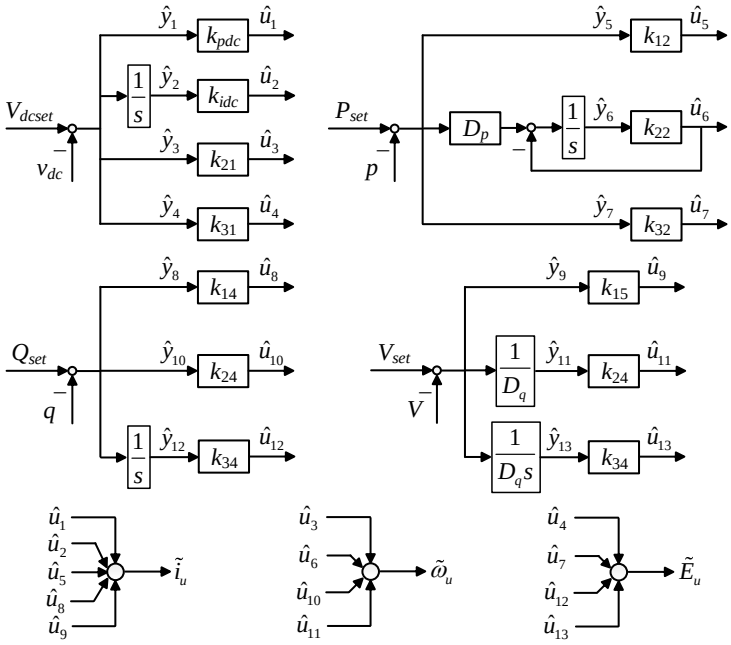

Fig. 5.5: Block diagram of proposed control transfer matrix. Source: [J6].

5.3.1 Design Setup and H_∞ Formulation

To tune the parameters of the control transfer matrix using H_∞ optimization, the following steps are applied

- Separate the parameters to be designed from the control transfer matrix as shown in Fig. 5.5, where vectors $\hat{\boldsymbol{y}}$ and $\hat{\boldsymbol{u}}$ are two intermediate vectors. Afterwards, there is

$$\hat{\boldsymbol{u}} = diag(k_{pdc}, k_{idc}, k_{21}, k_{31}, k_{12}, k_{22}, k_{32}, k_{14}, k_{15}, k_{24}\boldsymbol{I_2}, k_{34}\boldsymbol{I_2})\hat{\boldsymbol{y}} = \boldsymbol{K}\hat{\boldsymbol{y}} \tag{5.16}$$

  where $\boldsymbol{K}$ contains only the parameters to be designed.

- Define the input and output signals to perform the H_∞ synthesis. In this thesis, they are chosen as $\boldsymbol{w} = [P_{set}\ \omega_g]^T$ and $\boldsymbol{z} = [P_{set} - p\ p\ \omega\ q + V/D_q]^T$ to achieve good power tracking and synchronization ability.

- Collapse the close-loop system of Fig. 5.3 to get the standard model in the form of linear fractional transformation as shown in Fig. 5.6.

- Choose weighting functions $W_{ij}(s)$ to limit the disturbance responses $T_{ij}(s)$ from w_j to z_i. The chosen $W_{ij}(s)$ in this thesis will be given in Section 5.3.2.

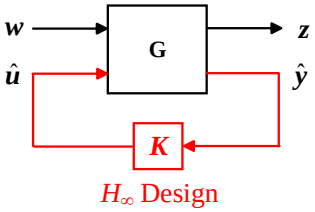

Fig. 5.6: Standard model in the form of linear fractional transformation. Source: [J6].

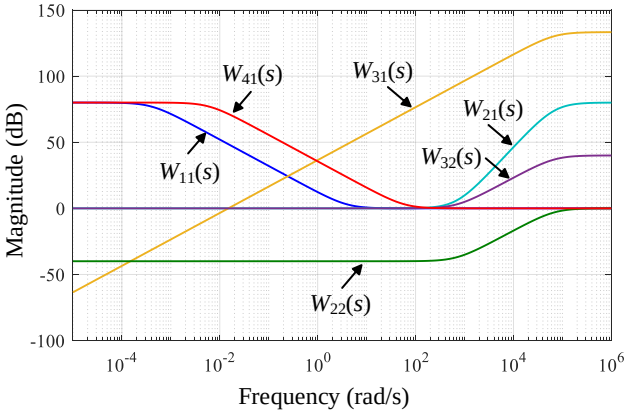

Fig. 5.7: Log-magnitude curves of chosen weighting functions. Source: [J6].

- Solve the following H_∞ optimization problem using the instructor *hinfstruct* in Matlab.

$$\min_K ||diag(W_{ij}(s)T_{ij}(s))||_\infty \tag{5.17}$$

5.3.2 Weighting Functions

The choices of the weighting functions reflect the requirements to the performance of the MIMO-SSSG. In this thesis, they are chosen based on the following requirements and their log-magnitude characteristics are shown in Fig. 5.7

- $W_{11}(s)$ should have large low-frequency gain to limit $T_{11}(s)$ in order to achieve small active power tracking, which is chosen as

$$W_{11}(s) = \frac{s + s_{11\_1}}{s + s_{11\_2}} \tag{5.18}$$

- $W_{21}(s)$ should have large high-frequency gain to limit $T_{21}(s)$ in order to suppress the high-frequency component in the active power tracking,

Table 5.2: Numbers Used in Weighting Functions

Symbol	Value	Symbol	Value	Symbol	Value
s_{11_1}	4	s_{11_2}	0.0004	T_{21_1}	1.447×10^{-3}
T_{21_2}	1.447×10^{-5}	k_{w22}	100	T_{22_1}	1.447×10^{-3}
T_{22_2}	1.447×10^{-5}	k_{w31}	0.015	T_{31_2}	1.447×10^{-5}
T_{32_1}	1.447×10^{-3}	T_{32_2}	1.447×10^{-5}	s_{41_1}	60
s_{41_2}	0.006				

which is chosen as

$$W_{21}(s) = \left(\frac{T_{21\_1}s + 1}{T_{21\_2}s + 1}\right)^2 \tag{5.19}$$

- $W_{22}(s)$ should have large high-frequency gain to limit $T_{22}(s)$ in order to suppress the high-frequency component in active power due to the disturbance in grid frequency, which is chosen as

$$W_{22}(s) = \frac{1}{k_{w22}} \times \frac{T_{22\_1}s + 1}{T_{22\_2}s + 1} \tag{5.20}$$

- $W_{31}(s)$ should have large high-frequency gain to limit $T_{31}(s)$ in order to suppress the RoCoF in the active power tracking, which is chosen as

$$W_{31}(s) = \frac{1}{k_{w31}} \times \frac{s}{T_{31\_2}s + 1} \tag{5.21}$$

- $W_{32}(s)$ should have large high-frequency gain to limit $T_{32}(s)$ in order to suppress the RoCoF in the synchronization, which is chosen as

$$W_{32}(s) = \frac{T_{32\_1}s + 1}{T_{32\_2}s + 1} \tag{5.22}$$

- $W_{41}(s)$ should have large low-frequency gain to limit $T_{41}(s)$ in order to keep the proposed controller without influencing the steady-state q-V droop characteristics, which is chosen as

$$W_{41} = \frac{s + s_{41\_1}}{s + s_{41\_2}} \tag{5.23}$$

The numbers in the weighting functions are summarized in Table 5.2.

Table 5.3: Parameters Used in MIMO-SSSG (Source: [J6])

Symbol	Description	Value
ω_n	nominal frequency	100π rad/s (1 p.u.)
S_n	nominal power	4 kW (1 p.u.)
V_n	nominal line-to-line RMS voltage	380 V (1 p.u.)
ω_g	grid frequency	1 p.u.
V_g	grid voltage	1 p.u.
L_s	line inductor	2 mH (0.017 p.u.)
R_s	line resistor	0.06 Ω (0.0017 p.u.)
C_f	filter capacitor	20 μF (0.23 p.u.)
L_f	filter inductor	2 mH (0.017 p.u.)
C_{dc}	DC capacitor	500 μF
D_p	droop coefficient of p-f regulation	0.01 p.u.
D_q	droop coefficient of q-V regulation	0.05 p.u.
P_{set}	Active power reference	0.5 p.u.
Q_{set}	Reactive power reference	0 p.u.
V_{set}	Voltage magnitude reference	1 p.u.
V_{dcset}	DC voltage reference	700 V

With the above weighting functions, the control parameters can be solved and then the proposed control transfer matrix is derived as

$$\mathbf{\Phi} = \begin{bmatrix} 120.224 + \frac{265.6217}{s} & -0.0019 & 0 & 0.1673 & -0.8274 \\ -0.8382 & \frac{0.017622}{s+1.7622} & 0 & 0 & 0 \\ -4.8977 & 0 & 0 & \frac{1.0844}{s} & \frac{21.6872}{s} \end{bmatrix} \tag{5.24}$$

The superior performance of the proposed MIMO-based control is verified by simulations in Matlab/Simulink with the parameters listed in Table 5.3. The results are shown in Fig. 5.8 and Fig. 5.9, where the studied disturbance are from P_{set} and ω_g, respectively. As seen, the performance of the traditional droop control and basic SSSG control (with the control matrix being (5.9)) has large oscillations. In comparison, the proposed control can provide smoother dynamics.

The performance of the proposed control is also experimentally using the setup shown in Fig. 1.9, where the results are shown in Fig. 5.10 and Fig. 5.11. It is worth mentioning that the basic SSSG cannot be stabilized in the experiments as shown in Fig. 5.12 due to various disturbances such as parameter errors and delays in the physical experimental system, although these oscillations can be damped in the simulations. This verifies the robustness of the

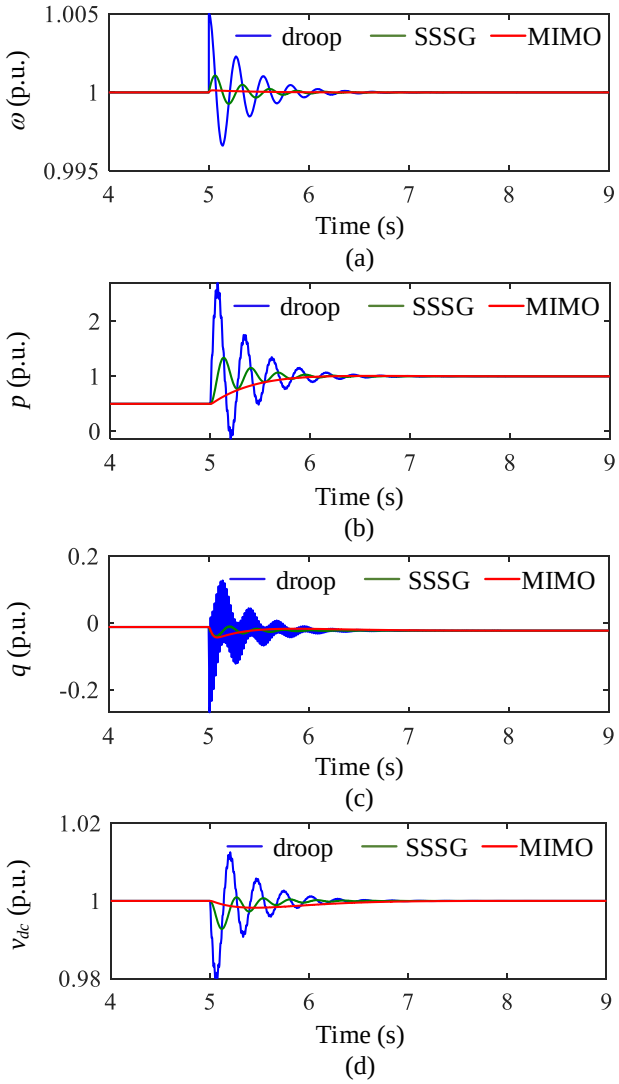

Fig. 5.8: Simulation results when P_{set} steps from 0.5 p.u. to 1 p.u. Source: [J6].

proposed MIMO-SSSG.

5.4 Summary

The MIMO-SSSG is proposed and designed in this chapter. A generalized configuration with a control transfer matrix for the grid-forming converter is proposed from the perspective of a MIMO system using modern control the-

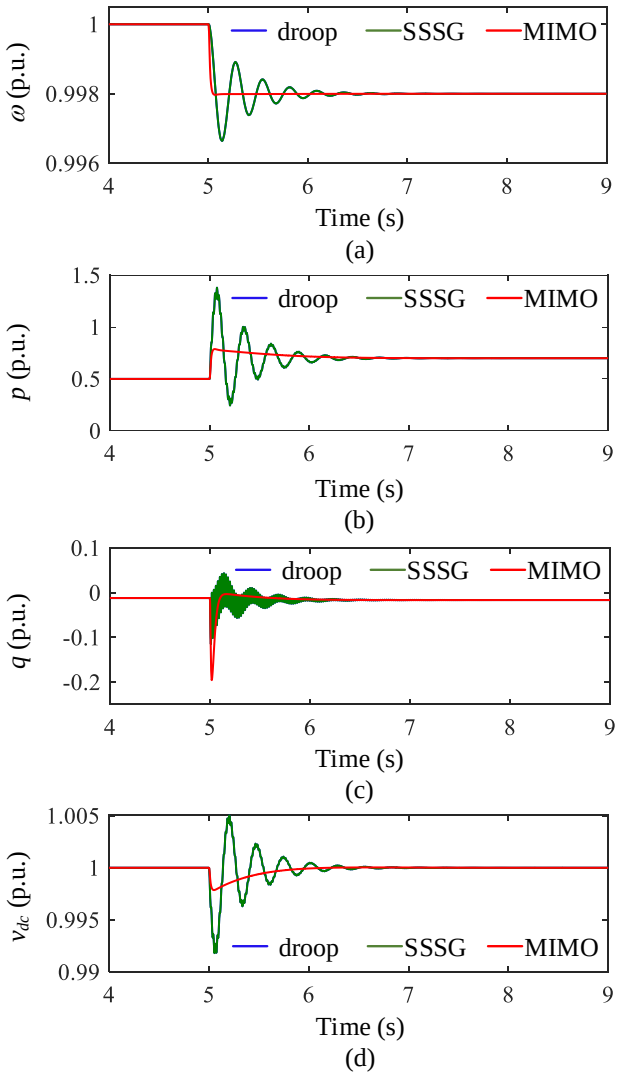

Fig. 5.9: Simulation results when w_g decreases from 50 Hz to 49.9 Hz. Source: [J6].

ory. It has indicated that the proposed configuration has several advantages such as unifying different grid-forming controls, inspiring new controls, etc. Thereafter, a new control transfer matrix is proposed to improve the performance of the SSSG by adding the coupling terms without using higher-order controllers. To cope with the multiple parameters in the proposed control, this chapter also presents in details how the parameters design can be transformed into a standard fixed structure using H_∞ optimization problem, which can address all the loops of AC and DC sides, and tune the parameters

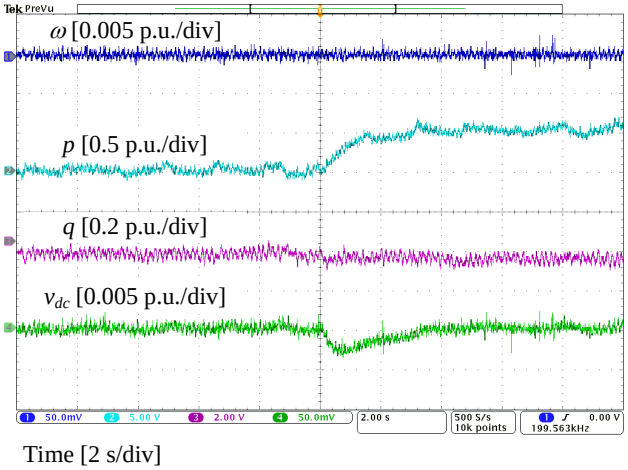

Fig. 5.10: Experimental results when P_{ref} steps from 0.5 p.u. to 1 p.u. Source: [J6].

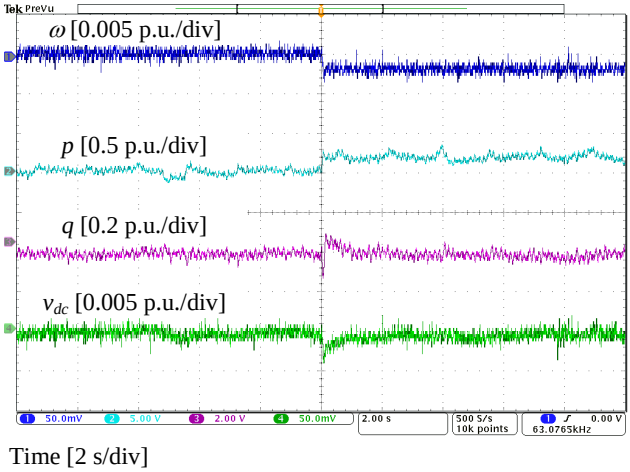

Fig. 5.11: Experimental results when w_g decreases from 50 Hz to 49.9 Hz. Source: [J6].

simultaneously. Simulations and experiments have been carried out, which demonstrate the superior and robust performance of the proposed MIMO-SSSG.

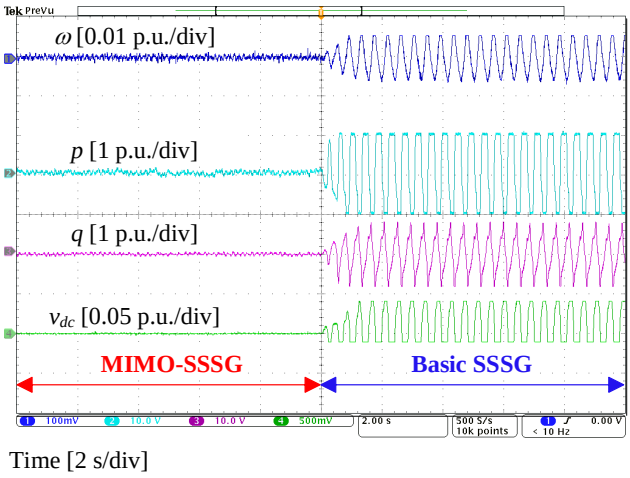

Fig. 5.12: Experimental results when the control method is changed from MIMO-SSSG to SSSG. Source: [J6].

Chapter 6

Conclusions

The results and outcomes of the Ph.D. study - *Modeling and control of solid-state synchronous generator* - are summarized in this chapter, where the main contributions of the research are underlined. Moreover, the possible future work is discussed at the end of the chapter.

6.1 Summary

The main research focus of this Ph.D. thesis is enabling a better integration of SSSGs into the future power-electronic-based power system. To this end, several challenging issues in respect to the SSSG have been studied, where the corresponding discussions and solutions have be proposed, especially by selecting proper control strategies. The research outcomes of the Ph.D. thesis is summarized as following.

In *Chapter 1*, the challenging issues about the integration of SSSGs into the future power system have been discussed, based on which the objectives of this Ph.D. thesis are proposed. On one hand, the dynamics of the power system with SSSGs are different compared to SGs due to their distinctions in modeling and application conditions. On the other hand, advanced control methods can provide superior and robust performance.

Although the main idea of the SSSG is to enable the IIGs to emulate actual SGs, different models may be used in all parts of the SSSG in the implementation. As a result, detailed dynamics among these models will be different as well. In *Chapter 2*, different models especially focusing on the virtual windings and virtual AVR are compared with each other and the SGs. In terms of the virtual windings, a 6th-order model wihch widely used in the SG and a 2nd-order model which widely used in the SSSG are considered by simulation studies for various operation conditions. With respect to the virtual AVR, three typical types are considered. Due to the distinctions between SGs

and SSSGs, some important dynamics such as electromechanical oscillation of the power system will be changed when more SGs are replaced by SSSGs. This issue is also coped with in *Chapter 2* by small-signal analysis, where the role of the participation factors is highlighted. Based on the analysis, a damping strategy is proposed by properly choosing the SGs to be replaced by the 2nd-order SSSGs, so the specific electromechanical modes can be damped.

In addition to the replacement by the SSSGs from the SGs, another feature for the future power system is more distributed as discussed in *Chapter 1*. Therefore, the connected power grid of the SSSG may not be strong, especially when applying it in a microgrid. To adapt this trend, *Chapter 3* proposes an equivalent coefficient model based on the small-signal analysis, which can be used to analyze the characteristics of the SSSG connected to a non-stiff grid by applying equivalent inertia, damping, and synchronizing coefficients. This model is an extension of the traditional Phillips-Heffron model used in analyzing a SMIB system. According to the proposed model, it is clear how the control and system parameters will affect the characteristics of a specific SSSG, e.g. the RoCoF at the beginning of a disturbance. In *Chapter 3*, the equivalent coefficient model is also used to derive the conditions for dynamic active power sharing and adaptively design the inertia constants with different disturbances.

Based on the basic SSSG, more favorable features are of interest to be added in the SSSG by proper controls in order to take fully advantages of the flexibility of the power converters. Although *Chapter 3* discusses the conditions of parameters matching to achieve dynamic active power sharing, they can hardly be met in practice. Therefore, damping the active power oscillations due to the mismatch of parameters is important, which is coped with in *Chapter 4*. The proposed method is based on the analysis that the active power can be controlled by the acceleration of the frequency. As a result, an additional damping is constructed by both terms of the acceleration feedback and disturbance suppression. Moreover, a small-signal analysis is provided to choose the parameters. It has been shown that the proposed method can well damp the active power oscillations. Another important feature is good transient angle stability. When an SSSG is connected in to a weak grid, the current limits may not be triggered after a voltage drop due to a large line impedance. Nevertheless, the basic SSSG may not guarantee a stable operation. A quantitative analysis on the impact of the internal voltage of the SSSG on the transient angle stability is carried out in *Chapter 4*, which proves the negative impact of the voltage control on the SSSG by decreasing the transmitted active power during the transient. Thereafter, an improved SSSG with enhanced transient angle stability is proposed by using the signal of the absolute value of acceleration power. A large-signal stability analysis is presented, which indicates that the proposed method is effective by decreasing the acceleration area while increasing the deceleration area.

Although the assumptions like ideal DC sources and decoupling different loops as SISO systems can simplify the analysis of the SSSG, it may sacrifice the potential performance as the useful information in the coupling terms are neglected. The possibility of providing a superior and robust performance by taking the SSSG as an MIMO system by considering both AC and DC dynamics is investigated in *Chapter 5*. Unlike from the perspective of emulating an SG, *Chapter 5* begins with focusing on the grid-forming converter, which is modeled by an MIMO system with three inputs and five outputs. A generalized configuration is proposed, where a control transfer matrix is used to construct a multivariable feedback control structure and unify various grid-forming control methods. This generalized configuration is then used to specifically establish a new MIMO-SSSG, where the couplings between AC and DC sides are explicitly considered by several simple P controllers. Furthermore, to cope with the multiple parameters, where the methods based on the classic control theory may not provide an optimal result, the tuning of the proposed MIMO-SSSG is transformed into a standard fix-structured H_∞ optimization problem. An example of choosing the weighting functions is also given in *Chapter 5*. Simulation and experimental results shows that the MIMO-SSSG can provide superior and robust performance.

6.2 Main Contributions

According to the research outcomes, the main contributions of the Ph.D. project are summarized as follows:

Comparison and analysis of solid-state SG with different modelings

- Different modeling methods of the SSSG especially virtual winding and virtual AVR are compared, which implies that a 2nd-order SSSG with droop-I control is simple but it has good performance.
- The impact on the electromechanical oscillation of the power system when the SGs are replaced by the SSSGs has been studied in details by small-signal analysis, which reveals the relationships among the significant states, electromechanical modes, and the damping provided by the SSSG.
- A simple damping method has been proposed to the electromechanical oscillations, which can be used to determine which SG should be replaced by an SSSG in order to damp a specified unwanted electromechanical mode.

Characteristics analysis of solid-state SG connected into a non-stiff grid

- The traditional Phillips-Heffron model used in SMIB system has been extended to an equivalent coefficient model used in a paralleled SSSGs system.
- How various control and system parameters influence the dynamics of the SSSG (e.g., RoCoF at the beginning of disturbances) is revealed, where both disturbances from the local load and set-point values are considered.
- The conditions to achieve dynamic active power sharing have been given.
- A modified inertia control is proposed, which has good performance responding to both disturbances from the local load and the set-point values.

Improved control of solid-state SG with additional functions

- An active power oscillation damping control for the SSSG is proposed, where a small-signal analysis has been performed for the parameters design.
- Impact of the virtual AVR on the transient angle stability of the SSSG has been quantitatively studied in details.
- An enhanced transient angle stability control is proposed, where a large-signal analysis has been performed to evaluate its effectiveness.

Multivariable feedback control of solid-state SG

- A new perspective from MIMO system to understand the SSSG has been discussed, where a generalized configuration of the grid-forming converter is proposed based on the multivariable feedback control.
- A new MIMO-SSSG has been proposed, which takes both AC and DC dynamics into consideration.
- The parameter design of the MIMO-SSSG is transformed into a standard fix-structured H_∞ optimization problem, where all the control parameters can be tuned simultaneously to give a superior and robust performance without using high-order control structure.

6.3 Future Work

Besides the studied issues in this Ph.D. project, there still are several unaddressed challenges, which are worth investigating as follows:

- This Ph.D. project only focuses on the control performance of the SSSG without considering the physical restraints. The limitations of the DC source such as energy density, power density, ect., should be considered in the future research. Also, the capability of providing high short-circuit current of the SG cannot be achieved naturally by the SSSG due to the limitation of the semiconductor devices, which is worth being researched how this could be achieved.

- Most of the studied systems in this Ph.D. project are single-machine or paralleled systems with grid-forming converters, future research should consider multi-machine systems with various types of source such as grid-forming converters, grid-following converters, SGs, etc., to be more practical - as it will be so in the future grid environment.

- In this Ph.D. project, the analysis on the proposed SSSGs with improved control is based on linearized system or on various assumptions to simplify the system. It is worth exploring advanced control and analysis methods based on the modern control theory to study the behaviors of the SSSG in a wider operating range.

- For the multivariable feedback control in this Ph.D. project, only a simple example is given to show the superior of the MIMO-based configuration. More studies can be carried out on how to design the control transfer matrix, where one of the promising directions is using non-linear controllers.

- This project mainly focuses on the characteristics of the power control loops in a low-frequency domain. However, the dynamics of the inner loops, the switching behavior of the power converter can also influence the performance of the SSSG. Therefore, more studies about the high-frequency behavior of the SSSG could be of interest.

- Although this Ph.D. project compares the dynamics between the SSSG and the SG, both of the studied system and operation conditions are limited. Meanwhile, there are some assumptions as the aforementioned discussion. Therefore, it does still not know whether an SSSG can get exact the same terminal characteristics in practice, which is an interesting topic for further research.

Bibliography

References

[1] J. Rocabert, A. Luna, F. Blaabjerg, and P. Rodríguez, "Control of power converters in AC microgrids," *IEEE Trans. Power Electron.*, vol. 27, no. 11, pp. 4734–4749, Nov. 2012.

[2] S. Eftekharnejad, V. Vittal, Heydt, B. Keel, and J. Loehr, "Impact of increased penetration of photovoltaic generation on power systems," *IEEE Trans. Power Syst.*, vol. 28, no. 2, pp. 893–901, May 2013.

[3] International Renewable Energy Agency, "Future of wind: Deployment, investment, technology, grid integration and socio-economic aspects," Tech. Rep., 2019.

[4] International Renewable Energy Agency, "Future of solar photovoltaic: Deployment, investment, technology, grid integration and socio-economic aspects," Tech. Rep., 2019.

[5] Danish Energy Agency, "Denmark's climate and energy outlook 2020," Tech. Rep., 2020.

[6] J. Fang, H. Li, Y. Tang, and F. Blaabjerg, "Distributed power system virtual inertia implemented by grid-connected power converters," *IEEE Trans. Power Electron.*, vol. 33, no. 10, pp. 8488–8499, Oct. 2018.

[7] J. Fang, H. Li, Y. Tang, and F. Blaabjerg, "On the inertia of future more-electronics power systems," *IEEE J. Emerg. Sel. Top. Power Electron.*, vol. 7, no. 4, pp. 2130–2146, Dec. 2019.

[8] G. Delille, B. Francois, and G. Malarange, "Dynamic frequency control support by energy storage to reduce the impact of wind and solar generation on isolated power system's inertia," *IEEE Trans. Sustain. Energy*, vol. 3, no. 4, pp. 931–939, Oct. 2012.

[9] A. Fernández-Guillamón, E. Gómez-Lázaro, E. Muljadi, and Á. Molina-García, "Power systems with high renewable energy sources: A review of inertia and frequency control strategies over time," *Renew. Sustain. Energy Rev.*, vol. 115, pp. 1–12, Nov. 2019.

[10] M. Karimi-Ghartemani, S. A. Khajehoddin, P. Piya, and M. Ebrahimi, "Universal controller for three-phase inverters in a microgrid," *IEEE J. Emerg. Sel. Top. Power Electron.*, vol. 4, no. 4, pp. 1342–1353, Dec. 2016.

[11] S. A. Khajehoddin, M. Karimi-Ghartemani, and M. Ebrahimi, "Grid-supporting inverters with improved dynamics," *IEEE Trans. Ind. Electron.*, vol. 66, no. 5, pp. 3655–3667, May 2019.

[12] L. Huang, H. Xin, and Z. Wang, "Damping low-frequency oscillations through VSC-HVdc stations operated as virtual synchronous machines," *IEEE Trans. Power Electron.*, vol. 34, no. 6, pp. 5803–5818, Jun. 2019.

[13] Xu She, A. Q. Huang, and R. Burgos, "Review of solid-state transformer technologies and their application in power distribution systems," *IEEE J. Emerg. Sel. Top. Power Electron.*, vol. 1, no. 3, pp. 186–198, Sep. 2013.

[14] H. Bevrani, T. Ise, and Y. Miura, "Virtual synchronous generators: A survey and new perspectives," *Int. J. Electr. Power Energy Syst.*, vol. 54, pp. 244–254, Jan. 2014.

[15] M. Chen and X. Xiao, "Hierarchical frequency control strategy of hybrid droop/VSG-based islanded microgrids," *Electr. Power Syst. Res.*, vol. 155, pp. 131–143, Feb. 2018.

[16] C. Li, Y. Li, Y. Cao, H. Zhu, C. Rehtanz, and U. Hager, "Virtual synchronous generator control for damping DC-side resonance of VSC-MTDC system," *IEEE J. Emerg. Sel. Top. Power Electron.*, vol. 6, no. 3, pp. 1054–1064, Sep. 2018.

[17] Q.-C. Zhong and G. Weiss, "Synchronverters: Inverters that mimic synchronous generators," *IEEE Trans. Ind. Electron.*, vol. 58, no. 4, pp. 1259–1267, Apr. 2011.

[18] V. Natarajan and G. Weiss, "Synchronverters with better stability due to virtual inductors, virtual capacitors, and anti-windup," *IEEE Trans. Ind. Electron.*, vol. 64, no. 7, pp. 5994–6004, Jul. 2017.

[19] H.-P. Beck and R. Hesse, "Virtual synchronous machine," in *2007 9th Int. Conf. Electr. Power Qual. Util.*, Barcelona, 2007, pp. 1–6.

[20] S. D'Arco, J. A. Suul, and O. B. Fosso, "A virtual synchronous machine implementation for distributed control of power converters in smartgrids," *Electr. Power Syst. Res.*, vol. 122, pp. 180–197, May 2015.

[21] K. Shi, W. Song, H. Ge, P. Xu, Y. Yang, and F. Blaabjerg, "Transient analysis of microgrids with parallel synchronous generators and virtual synchronous generators," *IEEE Trans. Energy Convers.*, vol. 35, no. 1, pp. 95–105, Mar. 2020.

[22] H. Alrajhi Alsiraji and R. El-Shatshat, "Comprehensive assessment of virtual synchronous machine based voltage source converter controllers," *IET Gener. Transm. Distrib.*, vol. 11, no. 7, pp. 1762–1769, May 2017.

[23] P. Tielens and D. Van Hertem, "The relevance of inertia in power systems," *Renew. Sustain. Energy Rev.*, vol. 55, no. 2016, pp. 999–1009, Mar. 2016.

[24] J. Liu, Y. Miura, H. Bevrani, and T. Ise, "Enhanced virtual synchronous generator control for parallel inverters in microgrids," *IEEE Trans. Smart Grid*, vol. 8, no. 5, pp. 2268–2277, Sep. 2017.

[25] W. Wu, L. Zhou, Y. Chen, A. Luo, Y. Dong, X. Zhou, Q. Xu, L. Yang, and J. M. Guerrero, "Sequence-impedance-based stability comparison between VSGs and traditional grid-connected inverters," *IEEE Trans. Power Electron.*, vol. 34, no. 1, pp. 46–52, Jan. 2019.

[26] Z. Shuai, C. Shen, X. Liu, Z. Li, and Z. J. Shen, "Transient angle stability of virtual synchronous generators using Lyapunov's direct method," *IEEE Trans. Smart Grid*, vol. 10, no. 4, pp. 4648–4661, Jul. 2019.

[27] J. Liu, Y. Miura, and T. Ise, "Comparison of dynamic characteristics between virtual synchronous generator and droop control in inverter-based distributed generators," *IEEE Trans. Power Electron.*, vol. 31, no. 5, pp. 3600–3611, May 2016.

[28] J. Alipoor, Y. Miura, and T. Ise, "Power system stabilization using virtual synchronous generator with alternating moment of inertia," *IEEE J. Emerg. Sel. Top. Power Electron.*, vol. 3, no. 2, pp. 451–458, Jun. 2015.

[29] S. D'Arco and J. A. Suul, "Equivalence of virtual synchronous machines and frequency-droops for converter-based microgrids," *IEEE Trans. Smart Grid*, vol. 5, no. 1, pp. 394–395, Jan. 2014.

[30] J. Meng, S. Chen, C. Zhang, X. Chen, Q.-C. Zhong, Z. Lv, and Q. Huang, "An improved synchronverter model and its dynamic behaviour comparison with synchronous generator," in *2nd IET Renew. Power Gener. Conf. (RPG 2013)*, Beijing, 2013, pp. 1–4.

[31] R. Hesse, D. Turschner, and H.-P. Beck, "Micro grid stabilization using the virtual synchronous machine (VISMA)," *Renew. Energy Power Qual. J.*, vol. 1, no. 7, pp. 676–681, Apr. 2009.

[32] Y. Chen, R. Hesse, D. Turschner, and H. P. Beck, "Dynamic properties of the virtual synchronous machine (VISMA)," *Renew. Energy Power Qual. J.*, vol. 1, no. 9, pp. 755–759, May 2011.

[33] Y. Chen, R. Hesse, D. Turschner, and H.-P. Beck, "Comparison of methods for implementing virtual synchronous machine on inverters," *Renew. Energy Power Qual. J.*, vol. 1, no. 10, pp. 734–739, Apr. 2012.

[34] M. Abuagreb, B. Ajao, H. Herbert, and B. K. Johnson, "Evaluation of virtual synchronous generator compared to synchronous generator," in *2020 IEEE Power Energy Soc. Innov. Smart Grid Technol. Conf.*, 2020, pp. 1–5.

[35] O. Mo, S. D'Arco, and J. A. Suul, "Evaluation of virtual synchronous machines with dynamic or quasi-stationary machine models," *IEEE Trans. Ind. Electron.*, vol. 64, no. 7, pp. 5952–5962, Jul. 2017.

[36] X. Meng, J. Liu, and Z. Liu, "A generalized droop control for grid-supporting inverter based on comparison between traditional droop control and virtual synchronous generator control," *IEEE Trans. Power Electron.*, vol. 34, no. 6, pp. 5416–5438, Jun. 2019.

[37] W. Du, Z. Chen, K. P. Schneider, R. H. Lasseter, S. Pushpak Nandanoori, F. K. Tuffner, and S. Kundu, "A comparative study of two widely used grid-forming droop controls on microgrid small-signal stability," *IEEE J. Emerg. Sel. Top. Power Electron.*, vol. 8, no. 2, pp. 963–975, 2020.

[38] J. Chen, M. Liu, and T. O'Donnell, "Replacement of synchronous generator by virtual synchronous generator in the conventional power system," in *2019 IEEE Power Energy Soc. Gen. Meet.*, vol. 3, 2019, pp. 1–5.

[39] Y. Hirase, K. Abe, K. Sugimoto, K. Sakimoto, H. Bevrani, and T. Ise, "A novel control approach for virtual synchronous generators to suppress frequency and voltage fluctuations in microgrids," *Appl. Energy*, vol. 210, pp. 699–710, Jan. 2018.

[40] W. Du, Q. Fu, and H. F. Wang, "Power system small-signal angular stability affected by virtual synchronous generators," *IEEE Trans. Power Syst.*, vol. 34, no. 4, pp. 3209–3219, Jul. 2019.

[41] J. M. Mauricio and A. E. Leon, "Improving small-signal stability of power systems with significant converter-interfaced generation," *IEEE Trans. Power Syst.*, vol. 35, no. 4, pp. 2904–2914, Jul. 2020.

[42] R. Rosso, S. Engelken, and M. Liserre, "Robust stability analysis of synchronverters operating in parallel," *IEEE Trans. Power Electron.*, vol. 34, no. 11, pp. 11 309–11 319, Nov. 2019.

[43] Z. Wang, F. Zhuo, H. Yi, J. Wu, F. Wang, and Z. Zeng, "Analysis of dynamic frequency performance among voltage-controlled inverters considering virtual inertia interaction in microgrid," *IEEE Trans. Ind. Appl.*, vol. 55, no. 4, pp. 4135–4144, Jul. 2019.

[44] Z. Wang, H. Yi, F. Zhuo, J. Wu, and C. Zhu, "Analysis of parameter influence on transient active power circulation among different generation units in microgrid," *IEEE Trans. Ind. Electron.*, vol. 68, no. 1, pp. 248–257, Jan. 2021.

[45] P. Kundur, *Power system stability and control*. McGraw-Hill, 1993.

[46] W. Gu, W. Liu, C. Shen, and Z. Wu, "Multi-stage underfrequency load shedding for islanded microgrid with equivalent inertia constant analysis," *Int. J. Electr. Power Energy Syst.*, vol. 46, no. 1, pp. 36–39, Mar. 2013.

[47] W. He, X. Yuan, and J. Hu, "Inertia provision and estimation of pll-based dfig wind turbines," *IEEE Trans. Power Syst.*, vol. 32, no. 1, pp. 510–521, Jan. 2017.

[48] R. K. Panda, A. Mohapatra, and S. C. Srivastava, "An effective inertia control scheme for solar pv systems with conventional dq controller," in *2018 IEEE Power Energy Soc. Gen. Meet.*, pp. 1–5.

[49] Y. Wu, D. Zhang, L. Xiong, S. Wang, Z. Xu, and Y. Zhang, "Modeling and mechanism investigation of inertia and damping issues for grid-tied PV generation systems with droop control," *Energies*, vol. 12, no. 10, pp. 1–17, May 2019.

[50] S. Tan, H. Geng, G. Yang, H. Wang, and F. Blaabjerg, "Modeling framework of voltage-source converters based on equivalence with synchronous generator," *J. Mod. Power Syst. Clean Energy*, vol. 6, no. 6, pp. 1291–1305, Nov. 2018.

[51] Power System Dynamic Performance Committee, "Stability definitions and characterization of dynamic behavior in systems with high penetration of power electronic interfaced technologies," Tech. Rep., 2020.

[52] Z. Shuai, W. Huang, Z. J. Shen, A. Luo, and Z. Tian, "Active power oscillation and suppression techniques between two parallel synchronverters during load fluctuations," *IEEE Trans. Power Electron.*, vol. 35, no. 4, pp. 4127–4142, Apr. 2020.

[53] M. Ebrahimi, S. A. Khajehoddin, and M. Karimi-Ghartemani, "An improved damping method for virtual synchronous machines," *IEEE Trans. Sustain. Energy*, vol. 10, no. 3, pp. 1491–1500, Jul. 2019.

[54] Y. Wang, J. Meng, X. Zhang, and L. Xu, "Control of PMSG-based wind turbines for system inertial response and power oscillation damping," *IEEE Trans. Sustain. Energy*, vol. 6, no. 2, pp. 565–574, Apr. 2015.

[55] J. Chen and T. O'Donnell, "Parameter constraints for virtual synchronous generator considering stability," *IEEE Trans. Power Syst.*, vol. 34, no. 3, pp. 2479–2481, May 2019.

[56] S. Dong and Y. C. Chen, "Adjusting synchronverter dynamic response speed via damping correction loop," *IEEE Trans. Energy Convers.*, vol. 32, no. 2, pp. 608–619, Jun. 2017.

[57] A. Adib and B. Mirafzal, "Virtual inductance for stable operation of grid-interactive voltage source inverters," *IEEE Trans. Ind. Electron.*, vol. 66, no. 8, pp. 6002–6011, Aug. 2019.

[58] A. Rodriguez-Cabero, J. Roldan-Perez, and M. Prodanovic, "Virtual impedance design considerations for virtual synchronous machines in weak grids," *IEEE J. Emerg. Sel. Top. Power Electron.*, vol. 8, no. 2, pp. 1477–1489, Jun. 2020.

[59] T. Shintai, Y. Miura, and T. Ise, "Oscillation damping of a distributed generator using a virtual synchronous generator," *IEEE Trans. Power Deliv.*, vol. 29, no. 2, pp. 668–676, Apr. 2014.

[60] D. Li, Q. Zhu, S. Lin, and X. Y. Bian, "A self-adaptive inertia and damping combination control of VSG to support frequency stability," *IEEE Trans. Energy Convers.*, vol. 32, no. 1, pp. 397–398, Mar. 2017.

[61] X. Zhang, F. Mao, H. Xu, F. Liu, and M. Li, "An optimal coordination control strategy of micro-grid inverter and energy storage based on variable virtual inertia and damping of vsg," *Chinese J. Electr. Eng.*, vol. 3, no. 3, pp. 25–33, Dec. 2017.

[62] M. Choopani, S. Hosseinain, and B. Vahidi, "A novel comprehensive method to enhance stability of multi-VSG grids," *Int. J. Electr. Power Energy Syst.*, vol. 104, pp. 502–514, Jan. 2019.

[63] H. Cheng, Z. Shuai, C. Shen, X. Liu, Z. Li, and Z. J. Shen, "Transient angle stability of paralleled synchronous and virtual synchronous generators in islanded microgrids," *IEEE Trans. Power Electron.*, vol. 35, no. 8, pp. 8751–8765, Aug. 2020.

[64] M. Choopani, S. H. Hosseinian, and B. Vahidi, "New transient stability and LVRT improvement of multi-VSG grids using the frequency of the center of inertia," *IEEE Trans. Power Syst.*, vol. 35, no. 1, pp. 527–538, Jan. 2020.

[65] X. Xiong, C. Wu, B. Hu, D. Pan, and F. Blaabjerg, "Transient damping method for improving the synchronization stability of virtual synchronous generators," *IEEE Trans. Power Electron.*, vol. 36, no. 7, pp. 7820–7831, Jul. 2021.

[66] X. Xiong, C. Wu, D. Pan, and F. Blaabjerg, "An improved synchronization stability method of virtual synchronous generators based on frequency feedforward on reactive power control loop," *IEEE Trans. Power Electron.*, 2021.

[67] H. Wu and X. Wang, "A mode-adaptive power-angle control method for transient stability enhancement of virtual synchronous generators," *IEEE J. Emerg. Sel. Top. Power Electron.*, vol. 8, no. 2, pp. 1034–1049, Jun. 2020.

[68] M. Ashabani and Y. A.-R. I. Mohamed, "Integrating VSCs to weak grids by nonlinear power damping controller with self-synchronization capability," *IEEE Trans. Power Syst.*, vol. 29, no. 2, pp. 805–814, Mar. 2014.

[69] V. Gevorgian, Y. Zhang, and E. Ela, "Investigating the impacts of wind generation participation in interconnection frequency response," *IEEE Trans. Sustain. Energy*, vol. 6, no. 3, pp. 1004–1012, Jul. 2015.

[70] J. Chen, M. Liu, F. Milano, and T. O'Donnell, "100% converter-interfaced generation using virtual synchronous generator control: A case study based on the irish system," *Electr. Power Syst. Res.*, vol. 187, pp. 1–10, Oct. 2020.

[71] S. D'Arco, J. A. Suul, and O. B. Fosso, "Small-signal modeling and parametric sensitivity of a virtual synchronous machine in islanded operation," *Int. J. Electr. Power Energy Syst.*, vol. 72, pp. 3–15, Nov. 2015.

[72] J. P. Radhakrishnan, "Transient stability analysis of grid with DFIG wind power plant," Master's thesis, May 2014.

[73] P. Demetriou, M. Asprou, J. Quiros-Tortos, and E. Kyriakides, "Dynamic IEEE test systems for transient analysis," *IEEE Syst. J.*, vol. 11, no. 4, pp. 2108–2117, Dec. 2017.

[74] Mathworks, "Performance of Three PSS for Interarea Oscillations." [Online]. Available: https://ch.mathworks.com/help/physmod/sps/ug/performance-of-three-pss-for-interarea-oscillations.html

[75] J. Ying, X. Yuan, J. Hu, and W. He, "Impact of inertia control of DFIG-based WT on electromechanical oscillation damping of SG," *IEEE Trans. Power Syst.*, vol. 33, no. 3, pp. 3450–3459, May 2018.

[76] IEEE Standard Association, *IEEE Std. 1547-2018. Standard for Interconnection and Interoperability of Distributed Energy Resources with Associated Electric Power Systems Interfaces*, 2018.

[77] A. D. Paquette, M. J. Reno, R. G. Harley, and D. M. Divan, "Sharing transient loads : Causes of unequal transient load sharing in islanded microgrid operation," *IEEE Ind. Appl. Mag.*, vol. 20, no. 2, pp. 23–34, Mar. 2014.

[78] H. Xu, X. Zhang, F. Liu, R. Shi, C. Yu, and R. Cao, "A reactive power sharing strategy of VSG based on virtual capacitor algorithm," *IEEE Trans. Ind. Electron.*, vol. 64, no. 9, pp. 7520–7531, Sep. 2017.

[79] H. Wu, X. Ruan, D. Yang, X. Chen, W. Zhao, Z. Lv, and Q.-C. Zhong, "Small-signal modeling and parameters design for virtual synchronous generators," *IEEE Trans. Ind. Electron.*, vol. 63, no. 7, pp. 4292–4303, Jul. 2016.

[80] D. Pan, X. Wang, F. Liu, and R. Shi, "Transient stability of voltage-source converters with grid-forming control: A design-oriented study," *IEEE J. Emerg. Sel. Top. Power Electron.*, vol. 8, no. 2, pp. 1019–1033, Jun. 2020.

[81] A. Tayyebi, D. Gross, A. Anta, F. Kupzog, and F. Dorfler, "Frequency stability of synchronous machines and grid-forming power converters," *IEEE J. Emerg. Sel. Top. Power Electron.*, vol. 8, no. 2, pp. 1004–1018, Jun. 2020.

[82] J. Liu, Y. Miura, H. Bevrani, and T. Ise, "A unified modeling method of virtual synchronous generator for multi-operation-mode analyses," *IEEE J. Emerg. Sel. Top. Power Electron.*, vol. 9, no. 2, pp. 2394–2409, Apr. 2021.

[83] L. Huang, H. Xin, H. Yang, Z. Wang, and H. Xie, "Interconnecting very weak AC systems by multiterminal VSC-HVDC links with a unified virtual synchronous control," *IEEE J. Emerg. Sel. Top. Power Electron.*, vol. 6, no. 3, pp. 1041–1053, Sep. 2018.

[84] J. Liu, Y. Miura, and T. Ise, "Fixed-parameter damping methods of virtual synchronous generator control using state feedback," *IEEE Access*, vol. 7, pp. 99 177–99 190, 2019.

Part II

Selected Publications

ISSN (online): 2446-1636
ISBN (online): 978-87-7210-854-4

AALBORG UNIVERSITY PRESS